A NEW LIQUID-VAPOR PHASE TRANSITION TECHNIQUE FOR THE LEVEL SET METHOD

A Dissertation
Presented to
The Academic Faculty

By
Nathaniel Ray Morgan

In Partial Fulfillment
Of the Requirements for the Degree
Doctor of Philosophy in Mechanical Engineering

Georgia Institute of Technology

May, 2005

A NEW LIQUID-VAPOR PHASE TRANSITION TECHNIQUE FOR THE LEVEL SET METHOD

Approved by:

Dr. Marc Smith, Chairman
George W. Woodruff
School of Mechanical Engineering
Georgia Institute of Technology

Dr. S. Mostafa Ghiaasiaan
George W. Woodruff
School of Mechanical Engineering
Georgia Institute of Technology

Dr. Fotis Sotiropoulos
George W. Woodruff
School of Mechanical Engineering
Georgia Institute of Technology

Dr. Peter Mucha
School of Mathematics
Georgia Institute of Technology

Dr. John Dolbow
School of Civil & Environmental Engineering
Duke University

Date Approved: April 04, 2005

To my family:

My wife, Celina Morgan

My daughter, Amelia Morgan

My father, Raymond Morgan

My mother, Virginia Morgan

My brother, Jonathan Morgan

ACKNOWLEDGMENTS

This work was supported by the Department of Energy Computational Science Graduate Fellowship Program of the Office of Scientific Computing and Office of Defense Programs in the Department of Energy under the contract DE-FG02-97ER25308.

TABLE OF CONTENTS

DEDICATIONS iii

ACKNOWLEDGMENTS iv

LIST OF TABLES viii

LISTS OF FIGURES ix

NOMENCLATURE xii

SUMMARY xvi

CHAPTER 1. INTRODUCTION 1

1.1. LIQUID-VAPOR PHASE TRANSITION 1

1.2. IMPROVING THE LEVEL SET METHOD 4

1.3 THESIS OVERVIEW 7

CHAPTER 2. A NEW LIQUID-VAPOR PHASE TRANSITION METHOD 9

2.1. OVERVIEW 9

2.2. GOVERNING EQUATIONS 10

2.3. INTERFACE JUMP CONDITIONS 12

2.4. THE LEVEL SET METHOD 15

2.5. ENERGY SOURCE TERM 18

2.6. INTERFACE BOUNDARY CONDITIONS 20

2.7. GHOST NODE CONSTRUCTION 26

2.8. NUMERICAL IMPLEMENTATION 31

2.9. SOLUTION STRATEGY 35

2.10. NUMERICAL TESTS 35

2.10.1. ONE-DIMENSIONAL TEST....36
2.10.2. TWO-DIMENSIONAL TEST....40
2.11. FILM BOILING SIMULATIONS....43
CHAPTER 3. IMPROVEMENTS TO THE LEVEL SET METHOD....49
3.1. OVERVIEW....49
3.2. THE PLIC VOLUME OF FLUID METHOD....50
3.3. THE COUPLED LEVEL SET VOLUME OF FLUID (CLSVOF) METHOD....52
3.3.1. ADVECTION FOR INCOMPRESSIBLE FLOWS....53
3.3.2. ADVECTION FOR FLOWS WITH PHASE CHANGE....57
3.3.3. CALCULATING VOLUME FRACTIONS....58
3.3.4. RECONSTRUCTING THE INTERFACE....61
3.3.5. IMPLEMENTING THE CLSVOF SCHEME....63
3.4. INITIAL VALUE TECHNIQUES FOR FORCING MASS CONSERVATION....64
3.4.1. A NEW APPROACH....66
3.5. ADVECTION TESTS....67
3.6. DROPLET TEST....72
3.7. FILM BOILING....74
CHAPTER 4. CONCLUSION....76
4.1. PHASE CHANGE SCHEME....76
4.2. IMPROVING THE LEVEL SET METHOD....78
4.3. CONTRIBUTIONS TO EXISTING NUMERICAL TECHNIQUES....79

4.4. FUTURE WORK.....81

APPENDIX A. HIGHER-ORDER EXTRAPOLATION.....82

REFERENCES 83

LIST OF TABLES

Table 2.1. Properties used with the film boiling simulation. 44

Table 3.1. The error after 1-rotation 70

Table 3.2. The error when the deformed circle returned to the starting location.....72

LIST OF FIGURES

Figure 2.1. A 1-D example of the discontinuous thermal conductivity across the interface (Left) and the corresponding temperature profiles (Right).....13

Figure 2.2. The extrapolation equation example.....19

Figure 2.3. The location where the immersed boundary conditions are applied.....20

Figure 2.4. The stencil used to apply immersed boundary conditions.....21

Figure 2.5. The pseudo code for the interface boundary conditions corresponding to cell based iteration.....24

Figure 2.6. The pseudo code for the interface boundary conditions corresponding to field based iteration.....24

Figure 2.7. The illustration above shows the ghost nodes for the vapor phase (black nodes) and the liquid phase (gray nodes), which are used to calculate the temperature gradient in the other respective phase.....28

Figure 2.8. The derivative stencil for constructing ghost nodes may require the temperature at another ghost node.....29

Figure 2.9. An example illustrating the stencils used to calculate the vapor temperature gradient (left) and the liquid temperature gradient (right); the vapor phase ghost nodes are indicated with arrows on the left side and no ghost nodes are required for the liquid phase in this example.....30

Figure 2.10. The computational grid used in this simulation, where the scalars are stored at the cell centers and the vector components are stored on the cell faces.....32

Figure 2.11. The liquid-vapor phase-change test problems - the left plot corresponds to the 1D numerical test, and the right plot corresponds to the 2D numerical test.....36

Figure 2.12. The interface position determined analytically and numerically using a 90x90 grid.....38

Figure 2.13. The L_2 error norm for the interface position as a function of the grid size for the 1D test problem.....39

Figure 2.14. The L_2 error norm for the temperature as a function of the grid size for the 1D test problem....39

Figure 2.15. The interface location at 2 seconds is shown on the top and the interface location at 3 seconds is shown on the bottom for a 90x90 grid; the dotted line corresponds to the initial position, the solid line corresponds to the numerical solution at the respective time, and the dashed line corresponds to the analytical solution at the respective time. 42

Figure 2.16. The L_2 error norm for the interface position as a function of the grid size for the 2D test problem 42

Figure 2.17. The L_2 error norm for the temperature as a function of the grid size for the 2D test problem....43

Figure 2.18. Film boiling simulation results at 0, 0.2, 0.25, and 0.3 seconds respectively, where the top row shows the temperature contours, and the bottom row shows the interface location and velocity field. 46

Figure 2.19. The heat transfer coefficient calculated by using the Berrenson correlation (horizontal line) and calculated numerically....47

Figure 2.20. Film boiling simulation results at 0, 0.2, 0.25, and 0.3 seconds respectively, where the top row shows the temperature contours, and the bottom row shows the interface location and velocity field. 48

Figure 3.1. The volume fraction flux, $G_{i+1/2}$, leaving the cell corresponds to the region, $\Delta\alpha\Delta\beta$, where the integral of the Heaviside function over the exit region corresponds to the shaded area. The letters l and v correspond to the liquid and vapor phases respectively. 55

Figure 3.2. A diagram illustrating the x-intercept, y-intercept, and z-intercept locations for the interface where the dimensions of the box are Δx by Δy by Δz....60

Figure 3.3. A diagram illustrating the integration path for finding the area enclosed by a polygon, where the numbers correspond to the vertexes; the dimensions of the box are Δx by Δy. 61

Figure 3.4. The results are shown at the starting location and after 1-rotation, where all the results correspond to a 100x100 mesh. 69

Figure 3.5. The results are shown after 500 steps forward in time and when the deformed circle returned to the starting location. 71

Figure 3.6. Droplet test results corresponding to the CLSVOF method (top row) and the level set method (bottom row). 73

Figure 3.7. Film boiling test results corresponding to the CLSVOF method (top row) and the level set method (bottom row). 75

NOMENCLATURE

A	Constant
$A_{polygon}$	Area of a polygon
α	Thermal diffusivity
β	Coefficients for the Runge-Kutta method
B	Constant
c	Specific heat at constant pressure
C	Constant
D	Difference Operator
Δ	Grid spacing
Δt	Time step
Δx	X-direction step size
Δy	Y-direction step size
ΔT	Change in temperature
δ_ε	Smeared delta function
δ	Interface position
e	Error velocity
ε	Half the smeared distance
F	Volume Fraction
ϕ	Level set function

$\bar{\phi}$	Linearized level set function
G	Flux
γ	Dummy variable
Γ_{MASS}	Mass source term
Γ_{ENERGY}	Energy source term
h	Enthalpy
h_{fg}	Enthalpy of vaporization
h_c	Heat transfer coefficient
H	Heaviside function
$\overline{H}$	Heaviside function constructed from linearized level set function
H_ε	Smeared Heaviside function
i	Index in x-direction
j	Index in y-direction
Ja	Jacob number
κ	Curvature
k	Thermal conductivity
λ	Solution to transcendental equation
$\vec{n}$	Normal vector
m''	Mass flux
M	Mass
μ	Viscosity
n	Time level
O	Order of Magnitude

P	Pressure
Pr	Prandtle number
$\vec{q}$	Heat flux vector
$\vec{r}$	Position vector
Re	Reynolds number
ρ	Density
s	Scalar variable
$S(\phi)$	Sign function
$S_\varepsilon(\phi)$	Smoothed sign function
σ	Surface tension
ψ	Distance to interface in normal direction
t	Time
T	Temperature
τ	Artificial time
$\underline{\underline{\tau}}$	Stress tensor
u	x-direction velocity
v	y-direction velocity
$\vec{V}$	Velocity vector

Subscripts

0	Prior to reinitializing the level set field
INT	Interface

GHOST	Ghost node
l	Liquid phase
pc	Phase Change
SAT	Saturation
WALL	Wall
v	Vapor phase
VOF	Volume of fluid

Superscripts

*	Fractional step time level
(l)	Liquid phase
m	Index
x+	Forward Difference in the x-direction
x-	Backward Difference in the y-direction
y+	Forward Difference in the y-direction
y-	Backward Difference in the y-direction
(v)	Vapor phase

SUMMARY

The level set method offers a simple and robust approach to modeling liquid-vapor interfaces that arise in boiling and condensing flows. The current liquid-vapor phase-transition techniques used with the level set method are not able to account for different thermal conductivities and specific heats in each respective phase, nor are they able to accurately account for latent heat absorption and release. This thesis presents a new level set based technique for liquid-vapor phase-transition that accounts for different material properties in each respective phase, such as thermal conductivity and specific heat, while maintaining the interface at the saturation temperature. The phase-transition technique is built on the ghost fluid framework coupled with the standard level set method. A new technique is presented for constructing ghost nodes that implicitly captures the immersed boundary conditions and is second order accurate. The method is tested against analytical solutions, and it is used to model film boiling. The new phase-transition technique will greatly assist efforts to accurately capture the physics of boiling and condensing flows.

In addition to presenting a new phase transition technique, several techniques are studied for fixing the volume loss problem associated with the level set method. Various ideas have been suggested to fix this problem. The coupled level set volume of fluid method (CLSVOF) forces the level set field to satisfy mass conservation by using the volume of fluid method (VOF). Another suggested technique is to solve an additional partial differential equation during the reinitialization process to minimize mass loss.

Multiple tests are performed and the results from the coupled level set volume of fluid method are compared with the level set method.

The coupled level set volume of fluid method is extended to work with flows that have phase change. The advection scheme is adapted to work with the new phase change scheme presented in this work, which allows it to handle dissimilar material properties in the respective phase, and capture the latent heat released or absorbed during phase transition. The coupled level set volume of fluid method fixes the mass loss problem that accompanies the level set method; likewise, the method provides an easy way to accurately calculate the curvature of an interface, which can be difficult with the volume of fluid method. A film boiling simulation is performed to illustrate the superior performance of the coupled level set volume of fluid approach over the level set method and the volume of fluid method.

CHAPTER 1
INTRODUCTION

1.1 Liquid-Vapor Phase Transition

Phase change problems are quite complicated and many questions concerning the underlying physics still exist. Many numerical techniques exist that can simulate multiphase flow problems such as front tracking [Tryggvason et. al. (2001)], volume of fluid (VOF) [(Rudman (1997)], and the level set method [Osher and Fedkiw (2001)]. Each technique offers benefits; as well as challenges. The level set method can implicitly handle bubble break up and merger in a simple and robust manner; in contrast, the Lagrangian approach can be cumbersome to use for merging and breaking interfaces. The work of Torres and Brackbill (2000), and Shin and Juric (2003) has greatly improved the Lagrangian approach and eliminated the problems arising in merging and breaking interfaces, but the methods are more complicated than the level set method. The simplicity of the level set method is a major reason why it is a great tool for modeling phase-transition flows.

Juric and Tryggvason (1998) developed a way to model liquid-vapor phase-transition in multiphase flow problems. Juric and Tryggvason (1998) showed that the liquid-vapor phase-transition could be modeled by adding a source term to the continuity equation; likewise, the energy equation could be modified with another source term to account for the adsorption and release of latent heat. Son and Dhir (1998) extended the liquid-vapor phase-transition technique to the level set framework, and Son (2001) further improved the technique in an attempt to account for more thermodynamic

properties of each phase. The technique suggested by Son and Dhir (1998) neglects the heat transfer in the liquid phase by setting the liquid thermal conductivity to infinity in their formulation. Likewise, a major limitation in the technique suggested by Son (2001) is the thermal conductivity in the vapor phase is equal to the thermal conductivity in the liquid phase, and the specific heat of the vapor phase is assumed to be zero. The motivation for making these assumptions was to guarantee that the liquid-vapor interface was at the saturation temperature corresponding to the Clausius-Clapeyron equation [Bejan (1997)] without resorting to the complicated Newton iteration algorithm used by Juric and Tryggvason (1998). The liquid-vapor phase-transition formulation currently used with the level set framework is severely limited in comparison to other liquid-vapor phase-change techniques.

Shin and Juric (2003) recently developed another liquid-vapor phase-transition technique for the front tracking method based on the work of Udaykumar et. al. (1999). Udaykumar et. al. (1999) developed a sharp interface method for solidification. Likewise, Welch and Wilson (2000) developed a liquid-vapor phase-transition technique for the volume of fluid method (VOF) following a similar concept. Both of these methods, Shin and Juric (2003) and Welch and Wilson (2000), simplified the interface physics, and assumed that the interface temperature corresponded to the saturation temperature at the pressure of the fluid. The method suggested by Udaykumar et. al. (1999) can be adapted to work with the level set method, but it is better suited for the front tracking technique. However, as will be shown later it is possible to develop a similar phase-transition technique for boiling and condensing flows using the ghost fluid

framework that accounts for absorption and liberation of latent heat and different material properties in each respective phase.

Fedkiw et. al. (1999) created the ghost fluid method (GFM) for modeling multimaterial flows. This method has since been applied to many computational problems including bubble dynamics [Kang et. al. (2000), Caiden (20001)] and solidification [Gibou et. al. (2003)]. The ghost fluid method models the interface in a sharp fashion unlike the standard level set method. The Navier-Stokes equations are modified to take into account the discontinuity in the viscous terms; likewise, the Pressure Poisson Equation is modified to account for the surface tension force [Liu et. al. (2000)]. In the case of solidification, the diffusion operator is modified in the energy equation to account for the discontinuity in the properties across the interface. In addition, the interface discontinuity is handled by satisfying the Rankine-Hugoniot jump conditions by propagating artificial values (ghost nodes) on either side of the interface. For Stefan problems, the ghost fluid method offers a simple way to handle a sharp interface [Osher and Fedkiw (2003)]. Therefore, the new liquid-vapor phase-transition method will implement the ghost fluid methodology for calculating the temperature gradient on the interface, which is required for calculating the mass source term in the continuity equation.

The new liquid-vapor phase-transition technique will treat the interface as being sharp when calculating the interface temperature gradients in the mass source term. However, the interface will be smeared over 3 nodes when calculating the surface tension body force and when calculating the properties of a cell, which follows the standard level set methodology. In other words, the proposed method will implement the

standard level set method, which smears the interface over 3 nodes, except for calculating the temperature gradients on the interface. This follows the work of Shin and Juric (2003) who treated the interface as being smeared over several nodes and used the sharp interface probing technique of Udaykumar et. al. (1999) to calculate the temperature gradients on the interface. The continuous surface force model suggested by Brackbill et. al. (1992) will be used to model the surface tension force. Using the ghost fluid method in conjunction with the level set method offers a simple and robust way to model boiling and condensation.

In this work, a new technique is presented for maintaining the interface at the saturation temperature. The technique enables the new phase transition technique to capture the latent heat released or absorbed from phase transition without resorting to the complicated Newton-Raphson iteration technique suggested by Juric and Tryggvason (1998). Likewise, a new technique is presented for constructing ghost nodes more accurately. The results from this research will improve the modeling capabilities of the level set method.

1.2 Improving the Level Set Method

The level set method is a robust and straightforward way to handle multi-material flows; however, it has the tendency to artificially move the interface, which causes loss of volume. Several authors have proposed techniques to fix the volume loss problem of the level set method. Bourlioux (1995) suggested one of the first ideas, which was to

couple the level set method with the volume of fluid method, which is termed – CLSVOF (coupled level set volume of fluid method). Chang et al (1996) suggested solving an initial value problem that shifts the interface to satisfy global volume conservation when reinitializing the level set field to a signed distance function. Likewise, Son (2001) followed the work of Chang et. al. (1996) and extended the idea to account for multiple interfaces and phase transition. In this work, the CLSVOF method and the initial value techniques are studied and the results are compared with the level set method.

Noh and Woodward (1976) developed one of the first volume tracking methods, which is called the simple line interface calculation (SLIC). The SLIC method advects the volume fraction in a directionally split algorithm, where the interface in a cell is reconstructed using a piecewise constant – a straight line that is parallel to a coordinate axis. Hirt and Nichols (1981) proposed the volume of fluid method (VOF), which follows the SLIC method and approximates the interface as a piecewise constant. The problem with the SLIC method, Hirt and Nichols (1981) scheme, and other first-order interface representations, is the interface is modeled in a stair-step fashion. Youngs (1982) improved the volume of fluid method by reconstructing the interface in a cell using piecewise linear lines. The method suggested by Youngs (1982), and the other VOF methods that represent the interface as piecewise linear, are referred to as piecewise linear calculation (PLIC) methods. There are various interface reconstruction techniques for the PLIC methods. Puckett (1991) created the least squares volume of fluid interface reconstruction algorithm (LVIRA), which reconstructs the interface by a minimization technique. Puckett et. al. (1997) gives a good overview of the LVIRA scheme.

Likewise, Rider and Kothe (1998) suggested another interface reconstruction technique for the PLIC method.

It can be challenging to determine the normal vector and the curvature from the discontinuous volume fraction fields. Rider and Kother (1998) give an overview of some of the techniques used for calculating the normal vector, and Brackbill et. al. (1992) discusses techniques for calculating the curvature. The normal vector is essential for reconstructing the interface in the PLIC methods. Likewise, the curvature is important in surface tension flows and other physical problems. In addition, the curvature involves second-order derivatives so it is more challenging to accurately calculate. The curvature is calculated by smoothing the volume fraction field; however, it is difficult to know how much smoothing is necessary. In contrast, the level set method does not have any difficulties with calculating the surface normal or curvature, since the level set field is maintained as a signed distance function from the interface. This was one of the reasons given by Sussman and Puckett (2000) for coupling the level set method with the VOF method. The coupled level set volume of fluid method (CLSVOF) fixes the volume loss problem of the level set method, while providing a way to calculate the surface normal and the curvature in an accurate manner. Several papers have been published that suggest techniques for improving the accuracy and efficiency of the CLSVOF method. Sussman (2003) developed a fully second-order discretization of the Navier-Stokes equations that implements the CLSVOF method. Likewise, Son (2003) derived useful analytical equations for the volume fractions of a cell and suggested a technique to reconstruct the interfaces in an efficient manner.

The purpose of this study is to investigate and present techniques for improving the level set method. The CLSVOF method studied in this work implements the standard numerical technique for reinitializing the level set field (Sussman 1994) to be a signed distance function from the interface, where Sussman and Puckett (2000) and Son (2003) used an exact technique. Standard advection tests are performed along with multiphase simulations. In addition, the CLSVOF is extended to handle phase change and the results are compared to the level set method. The level set method results in this study correspond to the fifth-order WENO advection scheme and the second-order ENO advection scheme. The results from this study will greatly improve the accuracy of the level set method for modeling multiphase flows including flows with phase change.

1.3 Thesis Overview

This thesis is broken up into four chapters where the first chapter gives a basic introduction, the second chapter addresses the new liquid-vapor phase transition method, the third chapter focuses on the mass conservation techniques for the level set method, and the forth chapter gives the final conclusion of this research.

The second chapter begins with an overview of the current techniques and then discusses the governing conservation equations. Next, the interface jump conditions are used to derive the continuity equation source term, which accounts for compressibility effects along the interface. After this section, the details of the level set method are discussed. Then, a new technique is presented for satisfying the interface boundary

condition, which is later modified to create a new ghost node construction technique. Finally, the new phase transition technique is tested against known analytical solutions and the Berrenson film boiling correlation.

The third chapter begins with an overview of the current techniques used to force the level set method to conserve mass. After the overview, the volume of fluid (VOF) method is discussed in greater detail. Then, the coupled level set volume of fluid (CLSVOF) method is presented for incompressible flows based on the standard level set reinitialization scheme. In addition, the CLSVOF method is extended to work with the new phase transition technique. Then, the concept behind the initial value techniques is discussed, and a comparison is made between the CLVOF method and the initial value techniques. Finally, several advection tests are performed with the CLSOVF method along with a droplet impact simulation and a film boiling simulation.

CHAPTER 2
A NEW LIQUID-VAPOR PHASE TRANSITION TECHNIQUE

2.1 Overview

A new liquid-vapor phase transition technique is presented that can handle dissimilar material properties in the respective phases, while maintaining the interface at the saturation temperature. Each phase is treated as an incompressible fluid except along the interface, where the compressibility effects are handled by placing a source term on the continuity equation [Juric and Tryggvason (1998)]. Likewise, a source term is placed in the energy equation to capture the latent heat, which forces the flow to be at the saturation temperature along the interface. In this work, the saturation temperature is maintained by solving an extrapolation equation in an iterative manner along the interface, which applies the interface boundary condition to the nodes next to the interface. In other words, a new iterative technique is presented for capturing the latent heat released or absorbed without resorting to the complicated Newton-Raphson iteration technique suggested by Juric and Tryggvason (1998).

The dissimilar temperature gradients across the interface are captured by constructing ghost nodes in the other respective phase. The ghost nodes allow the temperature gradient on the interface to be found without resorting to the probing techniques commonly used with Lagrangian front tracking techniques [Udaykumar (1999)]. The ghost nodes are constructed by extrapolating the temperature field across the interface in an iterative manner, which is similar to the technique used to apply the

interface boundary conditions. The new ghost node construction technique is shown to be second-order accurate and it easily works in multiple dimensions; moreover, the technique is extremely quick.

The new liquid-vapor phase transition technique is tested against two analytical problems. The first test is a one-dimensional phase change problem and the second is a two-dimensional phase change problem. The new technique is also used to simulate film boiling and the results are compared to the Berrenson correlation.

2.2 Governing Equations

The conservation of mass for the entire flow domain is given by Equation (2.1)

$$\frac{\partial \rho}{\partial t} + \nabla \bullet \left(\rho \vec{V}\right) = 0 \tag{2.1}$$

where ρ is the density, t is the time, $\vec{V}$ is the velocity field. The multiphase flow is modeled as two incompressible fluids except along the interface where phase transition occurs (Equation 2.2).

$$\nabla \bullet \vec{V}_l = 0 \tag{2.2a}$$

$$\nabla \bullet \vec{V}_v = 0 \tag{2.2b}$$

The velocity in the liquid phase is given by, $\vec{V}_l$, and the velocity in the vapor phase is given by, $\vec{V}_v$. The velocity field can be expressed in terms of the Heaviside function, H (Equation 2.3).

$$\vec{V} = \vec{V}_l H + \vec{V}_v (1 - H) \tag{2.3}$$

Taking the divergence of Equation (2.3) and substituting in the incompressibility relations (Equation 2.2) yields the conservation of mass equation for flows with phase change,

$$\nabla \bullet \vec{V} = (\vec{V}_l - \vec{V}_v) \bullet \nabla H \tag{2.4}$$

which can be expressed as,

$$\nabla \bullet \vec{V} = \Gamma_{MASS} . \tag{2.5}$$

The source term on the right side of the continuity equation accounts for the volume change that occurs during phase transition, and it is zero everywhere in the solution domain except on the interface [Juric and Tryggvason (1998)]. The jump in velocity is found by solving the Rankine-Hugoniot jump conditions across the interface. In addition, the source term is a function of the temperature field, so the ghost fluid method will be used to calculate temperature gradients on the interface.

The conservation of momentum for two-phase flow is shown by Equation (2.6)

$$\frac{\partial \vec{V}}{\partial t} + \vec{V} \bullet \nabla \vec{V} = -\frac{\nabla P}{\rho} + \vec{g} + \frac{\nabla \bullet \underline{\underline{\tau}}}{\rho} - \frac{\sigma \kappa \nabla H}{\rho} \tag{2.6a}$$

$$\underline{\underline{\tau}} = \mu\left(\nabla \vec{V} + \nabla \vec{V}^T\right) \tag{2.6b}$$

where P is the pressure, $\underline{\underline{\tau}}$ is the stress tensor, ρ is the density, μ is the viscosity, σ is the surface tension, κ is the curvature, and H is the Heaviside function. The body force term on the right side of the momentum equation corresponds to the continuous surface force model of Brackbill et. al. (1992). The continuity equation source term, Γ_{MASS}, and the surface tension body force term allow the phase transition problem to be formulated as a single phase, which greatly reduces the complexity.

The energy conservation equation is given by Equation (2.7),

$$\frac{\partial(cT)}{\partial t} + \vec{V} \bullet \nabla(cT) = \frac{1}{\rho}\nabla \bullet (k\nabla T) + \frac{1}{\rho}\Gamma_{ENERGY} \tag{2.7}$$

where Γ_{ENERGY} is a source term to account for the latent heat absorbed or released at the interface, c is the specific heat, and k is the thermal conductivity. The energy source term is zero everywhere in the solution domain except along the interface. The interface is smeared over several nodes, which follows the standard level set formulation.

2.3 Interface Jump Conditions

The properties across the phase front are discontinuous (Figure 2.1). The Rankine-Hugoniot jump conditions for the mass and energy conservation across the interface are respectively,

$$[[\rho(\vec{V} - \vec{V}_{INT})]] \bullet \vec{n} = 0 \tag{2.8}$$

$$[[\rho h(\vec{V} - \vec{V}_{INT})]] \bullet \vec{n} = -[[\vec{q}]] \bullet \vec{n} \tag{2.9}$$

where $[[\gamma]] = \gamma_l - \gamma_v$, $\vec{V}$ is the velocity of a phase, $\vec{V}_{INT}$ is the velocity of the interface, $\vec{q}$ is the heat flux vector, $\vec{n}$ is the normal vector, and h is the enthalpy of a phase.

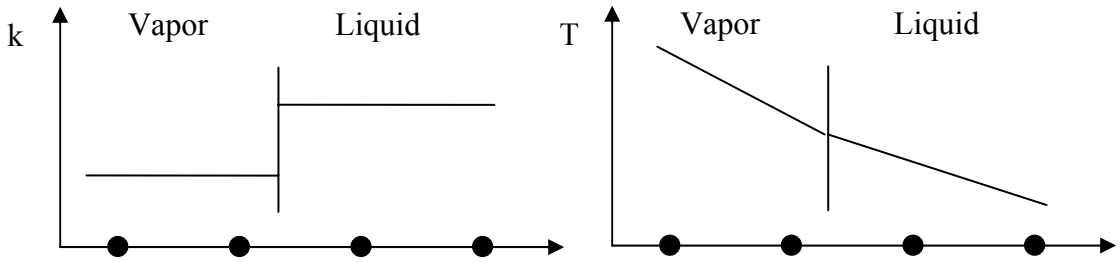

Figure 2.1 A 1-D example of the discontinuous thermal conductivity across the interface (Left) and the corresponding temperature profiles (Right)

Expanding Equations (2.8) and (2.9) and solving yields,

$$\rho_l\left(\vec{V}_l - \vec{V}_{INT}\right)\bullet\vec{n} = \frac{-(\vec{q}_v - \vec{q}_l)\bullet\vec{n}}{h_v - h_l} \tag{2.10a}$$

$$\rho_v\left(\vec{V}_v - \vec{V}_{INT}\right)\bullet\vec{n} = \frac{-(\vec{q}_v - \vec{q}_l)\bullet\vec{n}}{h_v - h_l} \tag{2.10b}$$

therefore,

$$\left(\vec{V}_l - \vec{V}_v\right)\bullet\vec{n} = \left(\frac{1}{\rho_v} - \frac{1}{\rho_l}\right)\frac{\left(\vec{q}_v - \vec{q}_l\right)\bullet\vec{n}}{h_v - h_l}. \tag{2.11}$$

The jump in velocity occurs across the interface, so Equation (2.11) is multiplied by the delta function, δ.

$$\left(\vec{V}_l - \vec{V}_v\right)\bullet\vec{n}\,\delta = \left(\frac{1}{\rho_v} - \frac{1}{\rho_l}\right)\frac{\left(-k_v\nabla T\big|_{INT}^{(v)} + k_l\nabla T\big|_{INT}^{(l)}\right)\bullet\vec{n}}{h_v - h_l}\delta. \tag{2.12}$$

The delta function can be expressed in terms of the Heaviside function

$$\nabla H = \vec{n}\,\delta, \tag{2.13}$$

so the source term for the continuity equation is,

$$\left(\vec{V}_l - \vec{V}_v\right) \bullet \vec{n} = \Gamma_{MASS} = \left(\frac{1}{\rho_v} - \frac{1}{\rho_l}\right) \frac{\left(-k_v \nabla T\big|_{INT}^{(v)} + k_l \nabla T\big|_{INT}^{(l)}\right)}{h_v - h_l} \bullet \nabla H \,. \tag{2.14}$$

In this study, Equation (2.14) is used to account for the volume change that occurs during phase transition. Welsh and Wilson (2000) used the relation in (2.14) to formulate a VOF approach; moreover, Osher and Fedkiw (2003) used a similar formulation for modeling Stefan problems using the ghost fluid method. In addition, Equation (2.14) is similar to the continuity equation source term suggested by Son and Dhir (1998).

The continuity equation source term used by Son and Dhir (1998) was,

$$\nabla \bullet \vec{V} = \left(\frac{1}{\rho_v} - \frac{1}{\rho_l}\right) \frac{-k_E \nabla T}{h_v - h_l} \bullet \nabla H_\varepsilon(\phi)\,, \tag{2.15}$$

where k_E is the effective thermal conductivity that corresponds to a constant temperature field in the liquid phase. The phase transition technique suggested by Son and Dhir (1998) forces the temperature in the liquid phase to be at the saturation temperature for all time; therefore, the liquid temperature gradient in Equation (2.15) is always zero. Likewise, the gradient operator in Equation (2.15) is approximated with a central difference. The technique suggested by Son and Dhir (1998) captures the latent heat absorbed or released by forcing the temperature in the liquid phase to always be at the saturation temperature. This thesis suggests a way to satisfy the interface temperature constraint without simplifying the physics.

2.4 The Level Set Method

Osher and Sethian (1988) initially proposed the level set method and since then it has been extended and applied to many computational problems [Sethian (1999), Osher and Fedkiw (2003)]. The level set method uses a higher dimensional function, ϕ, to represent the surface. The regions where the level set function is greater than zero correspond to the first material, the regions where the level set function is less than zero correspond to the second material, and the zero contour level represents the interface.

The level set field is advected on an Eulerian mesh using Equation (2.16),

$$\frac{\partial \phi}{\partial t} + \vec{V}_{INT} \bullet \nabla \phi = 0 \tag{2.16}$$

where $\vec{V}_{INT}$ is the characteristic velocity of the interface. If there were no phase transition, then the velocity of the interface would correspond to the velocity field. Using the expressions in (2.10a) and (2.10b), the velocity of the interface is given by,

$$\vec{V}_{INT} = \vec{V} + \frac{\vec{q}_v - \vec{q}_l}{\rho(h_v - h_l)} = \vec{V} + \frac{m''}{\rho} \tag{2.17a}$$

or

$$\vec{V}_{INT} = \vec{V} + \frac{\left(-k_v \nabla T\big|_{INT}^{(v)} + k_l \nabla T\big|_{INT}^{(l)}\right)}{\rho(h_v - h_l)} \tag{2.17b}$$

where *(v)* and *(l)* correspond to the vapor and liquid regions respectively, and m'' is the mass flux from phase transition.

After the interface is advected, a Heaviside function can be constructed from the level set field that selects the appropriate phase properties and implicitly captures the interface location. When the level set field is negative the Heaviside function is zero,

likewise, when the level set field is positive it is one. For stability purposes the Heaviside function is smeared over several nodes. The smooth Heaviside function and the smooth delta function are given by Equations (2.18) and (2.19) respectively.

$$H_\varepsilon(\phi) = \begin{cases} 0 & if \quad \phi < -\varepsilon \\ \frac{1}{2}\left(1 + \frac{\phi}{\varepsilon} + \frac{1}{\pi}\sin\left(\frac{\pi\phi}{\varepsilon}\right)\right), & if \quad |\phi| <= \varepsilon \\ 1 & if \quad \phi > \varepsilon \end{cases} \tag{2.18}$$

$$\delta_\varepsilon(\phi) = \begin{cases} 0 & if \quad \phi < -\varepsilon \\ \frac{1}{2\varepsilon}\left(1 + \cos\left(\frac{\pi\phi}{\varepsilon}\right)\right), & if \quad |\phi| <= \varepsilon \\ 0 & if \quad \phi > \varepsilon \end{cases} . \tag{2.19}$$

The term ε is usually set to one and a half times the grid size, $\frac{3}{2}\Delta$, in order to smooth the Heaviside and delta functions over three nodes; otherwise, the solution may be unstable, especially when coupled with the Navier-Stokes equations. The properties at a node can be represented as,

$$\gamma = \gamma_l H(\phi) + \gamma_v \left(1 - H(\phi)\right) \tag{2.20}$$

where γ_l and γ_v correspond to the properties of the respective phases such as density, specific heat, etc. The Heaviside function selects the property corresponding to the sign of the level set function; therefore, when $\phi>\varepsilon$ the property will be γ_l and when $\phi<-\varepsilon$ the property will be γ_v. Then in regions where $|\phi|<\varepsilon$, the property smoothly transitions between γ_l and γ_v over 3 grid nodes, which becomes a perfect step profile in the limit as the grid size goes to zero.

The level set function should be maintained as a signed distance function in order to improve the accuracy of the interface normal vector (Equation 2.21) and the curvature (Equation 2.22).

$$\vec{n} = \frac{\nabla \phi}{\left\| \nabla \phi \right\|_2} \tag{2.21}$$

$$\kappa = \nabla \bullet \vec{n} = \nabla \bullet \left(\frac{\nabla \phi}{\left\| \nabla \phi \right\|_2} \right) \tag{2.22}$$

The level set field will be a signed distance function from the interface when the 2-norm of the gradient is equal to 1 (Equation 2.23).

$$\left\| \nabla \phi \right\|_2 = 1 \tag{2.23}$$

As long as the level set field satisfies Equation (2.23) it will be maintained as a signed distance function. For a more extensive discussion of the distance function see Osher and Fedkiw (2003).

Sussman (1994) proposed an initial value technique to maintain the level set function as a sign distance function, which is shown by Equation (2.24).

$$\frac{\partial \phi}{\partial \tau} + S(\phi)\left(\left\| \nabla \phi \right\|_2 - 1 \right) = 0, \quad S(\phi) = \begin{cases} 1 & \phi > 0 \\ -1 & \phi < 0 \\ 0 & else \end{cases} \tag{2.24}$$

Equation (2.24) is a hyperbolic equation, where the sign function, $S(\phi)$, is the characteristic velocity and τ corresponds to artificial time. The sign function is smeared over several grid nodes for stability purposes. Sethian (1999) outlines a second-order method for solving Equation (2.24) to steady state in artificial time, based on the work of Osher and Sethian (1988). It is only necessary to solve Equation (2.24) for several steps

in artificial time, τ, after every real time step, t, to maintain the level set function as a signed distance function along the interface region.

2.5 Energy Source Term

The energy conservation equation is given by Equation (2.3). Discretizing the time derivative in Equation (2.7) yields,

$$T^{n+1} = \frac{(cT)^n}{c(\phi)^{n+1}} + \frac{\Delta t}{c(\phi)^{n+1}}\left(-\vec{V} \bullet \nabla\left(c(\phi)T\right)^n + \frac{\nabla \bullet (k(\phi)\nabla T)^n}{\rho(\phi)^n} + \frac{\Gamma_{ENERGY}^{n+1}}{\rho(\phi)^n} \right) \tag{2.25}$$

which can be written,

$$T^* = \frac{(cT)^n}{c(\phi)^{n+1}} + \frac{\Delta t}{c(\phi)^{n+1}}\left(-\vec{V} \bullet \nabla\left(c(\phi)T\right)^n + \frac{\nabla \bullet (k(\phi)\nabla T)^n}{\rho(\phi)^n} \right) \tag{2.26}$$

$$T^{n+1} = T^* + \Delta t\left(\frac{\Gamma_{ENERGY}^{n+1}}{\rho(\phi)^n c(\phi)^{n+1}} \right) \tag{2.27}$$

where T^* is the projected temperature field that neglects the latent heat absorbed or liberated, and T^{n+1} is the corrected temperature field. The energy source term in Equation (2.27) absorbs or releases energy, which forces the temperature field to remain at the saturation temperature along the interface. So Equation (2.27) can be written,

$$T^{n+1} = T^* + \Delta T_{PC}\,. \tag{2.28}$$

The temperature correction term, ΔT_{PC}, is zero everywhere except along the interface; therefore, the temperature at the projected time level, T^*, corresponds to the new time level, T^{n+1}, except along the interface. The source term in Equation (2.27) can be found

implicitly by using the Newton iteration technique suggested by Juric and Tryggvason (1998), or the change in temperature, ΔT_{PC}, in Equation (2.28) can be found that would produce the same effect as the source term.

The temperature correction term, ΔT_{PC} can be found implicitly by finding the temperature in the cells along the interface that correspond to the interface being at the saturation temperature,

$$T_{sat} = T_{i,j}^{n+1} + \psi \vec{n} \bullet \nabla T\Big|_{i,j}^{n+1} \tag{2.29}$$

where ψ is the distance from the interface to the cell in the normal direction, and the normal vector points into the liquid phase. Figure (2.2) shows a 1-D example of how Equation (2.29) forces the temperature field to satisfy the interface boundary condition.

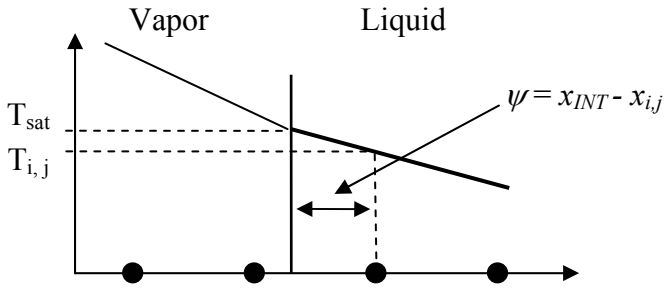

Figure 2.2 The extrapolation equation example

The temperature gradient in Equation (2.29) uses the temperature values at the new time level, *n+1*. The projected temperature values not near the interface correspond to the new temperature values, because the energy source term only corrects the temperature in cells along the interface. The temperature difference, $T_{i,j}^{n+1} - T_{i,j}^{*}$, corresponds to ΔT_{PC}. Equation (2.29) is indirectly finding the energy source term in Equation (2.25). The

corrected temperature field, T^{n+1} is used to calculate the continuity equation source term (Equation 2.14) at the next time level, $n+1$. The methodology outlined above uses Equation (2.26) to calculate the projected temperature field, and Equation (2.29) to account for the latent heat absorbed or liberated.

2.6 Interface Boundary Conditions

The level set framework can be used to represent sharp interfaces. The level set field is used as an indicator field where the liquid region corresponds to positive values and the vapor region corresponds to negative values; likewise, the zero contour level corresponds to the liquid-vapor interface. Since the interface, $\phi=0$, does not always pass through a node, the effect of the interfacial physics is extrapolated to the nearest node (Figure 2.3).

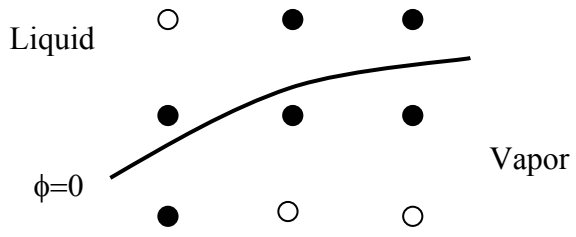

Figure 2.3 The location where the immersed boundary conditions are applied

The saturation temperature on the interface can be easily extrapolated to the nearest node by solving Equation (2.29) for the temperature at node i, j. Using the level set field, Equation (2.29) can be written,

$$T_{sat} = T_{i,j}^{n+1} - \phi_{i,j}\vec{n} \bullet \nabla T\Big|_{i,j}^{n+1}. \tag{2.30}$$

The level set field is maintained as a signed distance function from the interface; therefore, the absolute value of the level set function corresponds to the distance the node is from the interface in the normal direction. The negative sign in Equation (2.30) is the result of defining the vapor phase regions with negative values of ϕ. The temperature gradient is approximated using forward and backward differences, because the stencil should remain inside each respective phase (Figure 2.4).

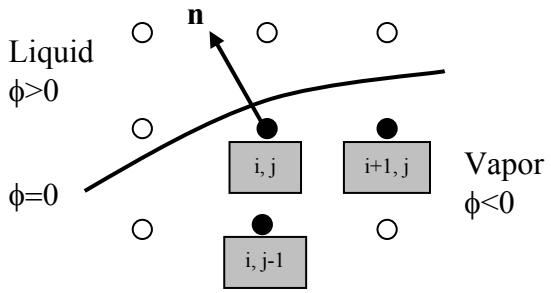

Figure 2.4 The stencil used to apply immersed boundary conditions

Substituting first-order forward and back difference relations into Equation (2.30) yields,

$$\begin{aligned} T_{sat} = T_{i,j}^{n+1} + \Bigg(& \min(0,-\phi_{i,j}^{n} n_{i,j}^{x}) \left(\frac{T_{i+1,j}^{n+1} - T_{i,j}^{n+1}}{\Delta x} \right) + \max(0,-\phi_{i,j}^{n} n_{i,j}^{x}) \left(\frac{T_{i,j}^{n+1} - T_{i-1,j}^{n+1}}{\Delta x} \right) + \\ & + \min(0,-\phi_{i,j}^{n} n_{i,j}^{y}) \left(\frac{T_{i,j+1}^{n+1} - T_{i,j}^{n+1}}{\Delta y} \right) + \max(0,-\phi_{i,j}^{n} n_{i,j}^{y}) \left(\frac{T_{i,j}^{n+1} - T_{i,j-1}^{n+1}}{\Delta y} \right) \Bigg) \end{aligned} \tag{2.31}$$

and solving for $T_{i,j}^{n+1}$ gives,

$$T_{i,j}^{n+1} = \frac{T_{sat} - B}{A} \tag{2.32a}$$

where,

$$A = 1 + \left(- \frac{\min(0, -\phi_{i,j}^{n} n_{i,j}^{x})}{\Delta x} + \frac{\max(0, -\phi_{i,j}^{n} n_{i,j}^{x})}{\Delta x} - \frac{\min(0, -\phi_{i,j}^{n} n_{i,j}^{y})}{\Delta y} + \frac{\max(0, -\phi_{i,j}^{n} n_{i,j}^{y})}{\Delta y} \right) \tag{2.32b}$$

$$B = \left(\frac{\min(0, -\phi_{i,j}^{n} n_{i,j}^{x})}{\Delta x} T_{i+1,j}^{n+1} - \frac{\max(0, -\phi_{i,j}^{n} n_{i,j}^{x})}{\Delta x} T_{i-1,j}^{n+1} + \frac{\min(0, -\phi_{i,j}^{n} n_{i,j}^{y})}{\Delta y} T_{i,j+1}^{n+1} - \frac{\max(0, -\phi_{i,j}^{n} n_{i,j}^{y})}{\Delta y} T_{i,j-1}^{n+1} \right). \tag{2.32c}$$

Only the temperature values along the interface are corrected; as a result, all the projected temperature values in the cells away from the interface correspond to the *n+1* time level. Thus, the only unknowns are the temperature values in the cells along the interface. The normal vector in the extrapolation equation is given by Equation (2.21). The *min* and *max* functions are implemented to ensure the derivative stencil only uses information from the correct phase. The extrapolation formula (Equation 2.32) is used for both phases near the interface. In addition, the interface temperature is equal to the saturation temperature at the system pressure, P_{∞}.

$$T_{SAT} = T_{SAT}(P_{\infty}) \tag{2.33}$$

The extrapolation equation may require the temperature at the new time level when calculating the temperature gradient; as a result, an iteration process is necessary for determining the new temperature. Two approaches were studied, where each approach is based on the Picard iteration method. Both schemes involve placing

Equation (2.32) in a loop and iterating (Equation 2.34a) until the difference between the old and the new temperature values (Equation 2.34b) are less than a specified tolerance.

$$T^{m+1} = \frac{T_{sat} - B(T^m)}{A(T^m)} \tag{2.34a}$$

$$Err = \max\left(\left|T_{i,j}^{new} - T_{i,j}^{old}\right|\right) \tag{2.34b}$$

The scheme above typically converged in a couple of iterations. As an example, each iteration reduced the error by at least 1-order of magnitude for the test problems discussed later in the paper. Likewise, for the film boiling simulations it usually required less than 20 iterations to reach a tolerance of 10^{-16}. In addition, Equation (2.34) is only solved along the interface, so the iteration procedure had no noticeable effect on the speed of the code with the grid sizes used in this study.

The iteration technique shown in Equation (2.34) can be continually updated with new information, which corresponds to the first solution approach; or the data could be updated after every value at the $m+1$ level is known, which corresponds to the second solution approach. The second solution method updates the entire field instead of the individual cells. Figure (2.5) and (2.6) illustrates how the first and second solution method works respectively.

whileloop *err>tol*
loop (i=1…endi)
loop (j=1…endj)

$$T_{i,j} = \frac{T_{sat} - B(T_{i,j})}{A(T_{i,j})}$$

end
end

$$err = \max\left(\left|T_{i,j} - T_{i,j}^{old}\right|\right)$$

endwhile

Figure 2.5 The pseudo code for the interface boundary conditions corresponding to cell based iteration

whileloop *err>tol*
loop (i=1…endi)
loop (j=1…endj)

$$T_{i,j}^{new} = \frac{T_{sat} - B(T_{i,j}^{old})}{A(T_{i,j}^{old})}$$

end
end

$$err = \max\left(\left|T_{i,j}^{new} - T_{i,j}^{old}\right|\right)$$

$$T^{old} = T^{new}$$

endwhile

Figure 2.6 The pseudo code for the interface boundary conditions corresponding to field based iteration

The second approach, which updated the entire field, produced the best results, because this approach used the same temperature field data to calculate the next iteration level. However, on occasion this approach would stall when the error (Equation 2.34b) was on the order of 10^{-16} , (using a machine with a sufficient number of bits) where the first approach never experienced this problem. In addition, the first approach would converge much faster, but in some simulations the solution would loose symmetry after

numerous time steps, Δt. In this study, the second approach was used in order to preserve the symmetry of the problem.

The method suggested for applying the interface temperature boundary conditions is second-order accurate. The accuracy can be calculated by multiplying the Taylor-Series expansion of the backward difference operator by the absolute value of ϕ.

$$\left|\phi_i\right|\left(\frac{T_i - T_{i-1}}{\Delta x}\right) = \left|\phi_i\right|\left(\frac{\partial T}{\partial x}\right)_i - \left|\phi_i\right|\left(\frac{\Delta x}{2}\right)\left(\frac{d^2 T}{dx^2}\right)_i + \ldots \tag{2.35}$$

Since $0 < \left|\phi_i\right| < \Delta x$ along the interface, then it easily follows that,

$$\left|\phi_i\right|\left(\frac{T_i - T_{i-1}}{\Delta x}\right) = \left|\phi_i\right|\left(\frac{\partial T}{\partial x}\right)_i + O\left(\Delta x^2\right). \tag{2.36}$$

Numerical tests at the end of this paper also verify that the technique is second-order accurate. It should be noted that the method has a tendency to produce errors in the curvature of the interface that decay as the square of the grid size. If a greater degree of accuracy is required, then higher-order difference schemes can be implemented, but care must be used for small bubbles because the derivative stencil may go into the other phase. In addition, higher-order terms can be included in the extrapolation formula to improve the interface accuracy. Appendix (A) shows the extrapolation equation corresponding to second-order differences.

2.7 Ghost Node Construction

The continuity equation source term (Equation 2.14) requires the gradient of the temperature to be known on both sides of the interface. Clearly, the temperature on the interface is equal to the saturation temperature, but the gradients on the vapor side and the liquid side are not equal (Figure 2.1); therefore, a ghost fluid formulation is used to calculate the gradient. Fedkiw et. al. (1999) suggested a technique for determining the ghost node values in the vapor phase and the liquid phase, which are shown by Equation (2.37a) and Equation (2.37b) respectively. Equation (2.37a) and (2.37b) are the standard first-order wave equations so they just advect the information in the normal direction.

$$\frac{dT_{GHOST}^{(v)}}{d\tau} + \vec{n} \bullet \nabla T_{GHOST}^{(v)} = 0 \tag{2.37a}$$

$$\frac{dT_{GHOST}^{(l)}}{d\tau} - \vec{n} \bullet \nabla T_{GHOST}^{(l)} = 0 \tag{2.37b}$$

The idea is to solve Equations (2.37a) and (2.37b) for several artificial time steps, τ, to populate values on either side of the interface depending on the derivative stencil used for the temperature gradient. One problem with using this proposed technique for a phase change formulation is the temperature values are only translated from one location to another, thus the gradient of the temperature is never taken into account. The justification for translating the temperature values is to prevent spurious oscillations from occurring, also known as the isobaric fix [Fedkiw et. al. (1999)]. Since the liquid-vapor phase change scheme is designed for two incompressible phases, the isobaric fix should not be necessary.

A better way to construct ghost node values for phase transition would be to take into account the gradient and not just translate information across the interface. Equation

(2.26) is an extrapolation formulation that accounts for the temperature gradient; therefore, just multiply the normal vector components in Equations (2.30) - (2.32) by a negative sign and information will be extrapolated across the interface in the normal direction. Currently, Equation (2.30) is formulated to extrapolate information away from the interface into the phase, not across the interface into the other phase. Therefore, an easy way to construct ghost node values is given by Equation (2.38)

$$T_{GHOST\,i,j} = \frac{T_{sat} - B}{A} \tag{2.38a}$$

where the new coefficients are,

$$A = 1 + \left(-\frac{\min(0, \phi_{i,j} n^x_{i,j})}{\Delta x} + \frac{\max(0, \phi_{i,j} n^x_{i,j})}{\Delta x} - \frac{\min(0, \phi_{i,j} n^y_{i,j})}{\Delta y} + \frac{\max(0, \phi_{i,j} n^y_{i,j})}{\Delta y} \right) \tag{2.38b}$$

$$B = \left(\frac{\min(0, \phi_{i,j} n^x_{i,j})}{\Delta x} T_{i+1,j} - \frac{\max(0, \phi_{i,j} n^x_{i,j})}{\Delta x} T_{i-1,j} + \frac{\min(0, \phi_{i,j} n^y_{i,j})}{\Delta y} T_{i,j+1} - \frac{\max(0, \phi_{i,j} n^y_{i,j})}{\Delta y} T_{i,j-1} \right). \tag{2.38c}$$

One benefit of using Equation (2.38) is the ghost nodes are constructed to implicitly capture the immersed boundary conditions on the interface; moreover, the interface location is also implicitly taken into account so no additional interpolation algorithms are necessary.

The ghost node values are only needed next to the interface so it is not necessary to solve Equation (2.38) over the entire domain. Figure (2.7) illustrates the location of the vapor phase and liquid phase ghost nodes respectively if first-order forward and backward difference operators are used for the temperature gradient. If second-order

difference operators are used, then multiple layers of ghost nodes must be extrapolated on either side of the interface. In addition, it is necessary to perform several iterations when constructing the ghost nodes, because the derivative stencil may require a neighboring ghost node temperature value. Figure (2.8) illustrates an example of how the derivative stencil in Equation (2.38) may need another ghost node; thus requiring an iterative process. The ghost node construction process would usually converge in a few iterations. Moreover, the iteration process requires very little effort since the ghost nodes are only constructed next to the interface. Basically, the construction algorithm was placed in a loop that would continue until the change in the ghost node values was less than a specified tolerance. The iteration method used was identical to techniques used to apply the interface boundary conditions. For the two-dimensional test problem discussed later, it usually required about 9 iterations to reach a tolerance of 10^{-16} for 3 layers of ghost nodes on both sides of the interface. Likewise, for the film boiling simulation discussed later it usually required between 4 and 20 iterations to reach an error less than 10^{-16} for 3 layers of ghost nodes. The ghost node construction process had little effect on the speed of the code; however, the number of iterations will increase as the number of nodes increases.

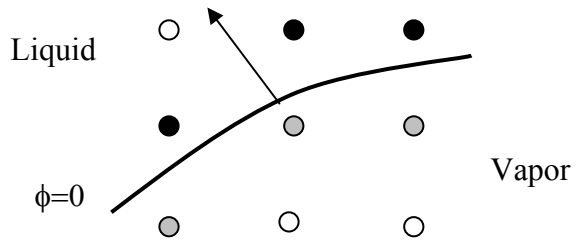

Figure 2.7 The illustration above shows the ghost nodes for the vapor phase (black nodes) and the liquid phase (gray nodes), which are used to calculate the temperature gradient in the other respective phase.

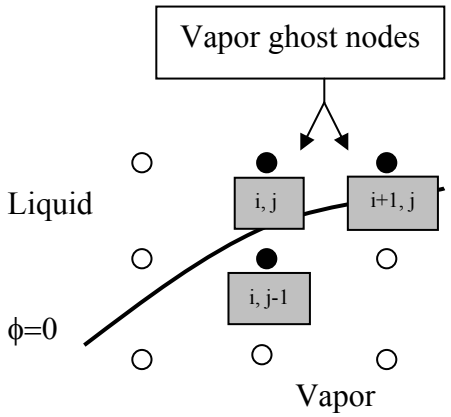

Figure 2.8 The derivative stencil for constructing ghost nodes may require the temperature at another ghost node.

After the ghost node values are known, it is possible to calculate the temperature gradients in the normal direction for the vapor and liquid phases using Equation (2.39a) and Equation (1.39b) respectively,

$$\vec{n} \bullet \nabla T^{(v)} = \left(\min(0, n^x) D^{x+} T^{(v)} + \max(0, n^x) D^{x-} T^{(v)} + \min(0, n^y) D^{y+} T^{(v)} + \max(0, n^y) D^{y-} T^{(v)}\right) \tag{2.39a}$$

$$\vec{n} \bullet \nabla T^{(l)} = \left(\min(0, -n^x) D^{x+} T^{(l)} + \max(0, -n^x) D^{x-} T^{(l)} + \min(0, -n^y) D^{y+} T^{(l)} + \max(0, -n^y) D^{y-} T^{(l)}\right) \tag{2.39b}$$

where, D^{x+}, D^{x-}, D^{y+}, and D^{y-} are the forward and backward difference operators in the x and y directions respectively. The difference operators use the ghost nodes when calculating the temperature gradients in the other phase, and Figure (2.9) illustrates an example. If higher-order difference operators are used, then it is important to construct a sufficient number of ghost nodes. The ghost node locations shown in Figure (2.9) correspond to first-order forward and backward difference operators; therefore, second-order forward and backward difference operators for the temperature gradient require 2 layers.

A benefit of the technique outlined above is the ability to find the temperature gradient on the interface in the normal direction without resorting to the complicated interpolation techniques commonly used in sharp interface Lagrangian methods [Udaykumar (1999), Balaras (2004), and Gilmanov et. al. (2003)]. The technique is trivial in 3 dimensions and requires very little computing effort. A higher-order method is simple, just use the appropriate forward and backward difference operators in Equation (2.39) and extrapolate a sufficient number of ghost nodes.

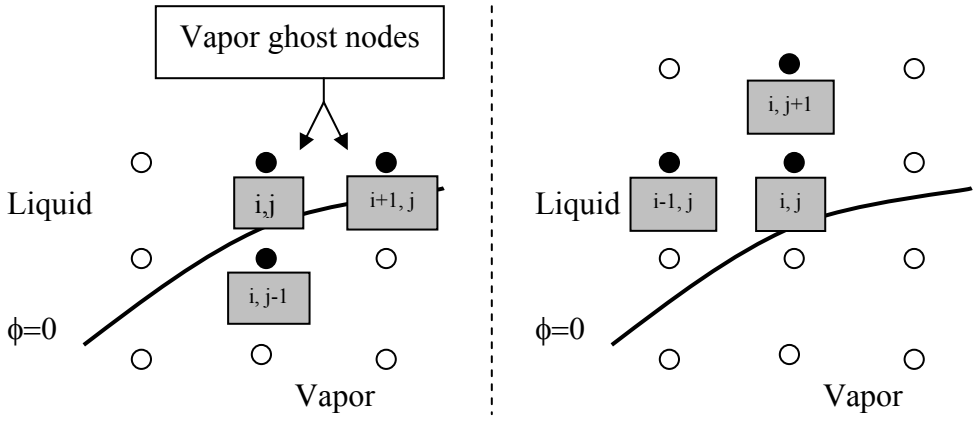

Figure 2.9 **An example illustrating the derivative stencils used to calculate the temperature gradient on the interface at the i,j node for the respective phases. The vapor temperature gradient is shown on the left and the liquid temperature gradient is shown on the right. The vapor phase ghost nodes are indicated with arrows on the left side and no ghost nodes are required for the liquid phase in this example.**

2.8 Numerical Implementation

The Navier-Stokes equations are solved using the projection method suggested by Chorin (1968). The method works by first calculating a fractional velocity, then the pressure at the next time level is calculated that ensures the velocity field satisfies the continuity equation. The projection step is shown by Equation (2.40),

$$\frac{\vec{V}^* - \vec{V}^n}{\Delta t} + \left(\vec{V}^n \bullet \nabla\right)\vec{V}^n = \frac{\left(\nabla \bullet \underline{\underline{\tau}}^n\right)}{\rho(\phi)} + \vec{g} - \frac{\sigma\kappa^n \nabla H^n}{\rho(\phi)} \tag{2.40}$$

and the correction step is shown by Equation (2.41),

$$\frac{\vec{V}^{n+1} - \vec{V}^*}{\Delta t} + \frac{\nabla p^{n+1}}{\rho(\phi)} = 0\,. \tag{2.41}$$

The pressure at the next time level, P^{n+1}, is found by taking the divergence of correction step (Equation 2.41), and using the continuity equation (Equation 2.5), which yields the pressure Poisson equation (PPE) (Equation 2.42).

$$\nabla \bullet \left(\frac{\nabla P^{n+1}}{\rho(\phi)} \right) = \frac{\nabla \bullet \vec{V}^* - \Gamma_{MASS}^{n+1}}{\Delta t} \tag{2.42}$$

The velocity components are stored on the cell faces and the pressure is stored at the cell center, which corresponds to the MAC grid [Harlow and Welsh (1965)]. Therefore, the projection and correction equations are solved on the cell faces and the pressure Poisson equation is solved at the cell centers. A preconditioned conjugate gradient (PCG) method is used to solve the pressure Poisson equation. Kelly (1995) and Golub and Van Loan (1983) give an in depth discussion of the PCG method. All the spatial derivatives in the Navier-Stokes equations are approximated with second-order central differences. Figure (2.10) illustrates the MAC grid, where the scalar values are stored at the cell

centers and the velocities components are stored on the cell faces. The velocity field is second-order accurate in space and first-order accurate in time. The pressure is also second-order accurate in space and first-order accurate in time.

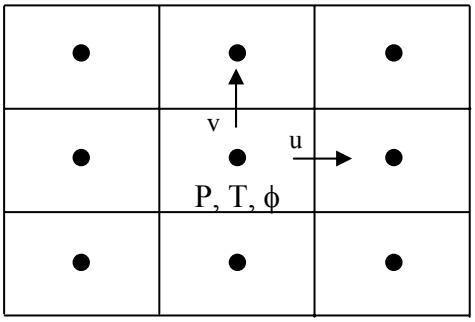

Figure 2.10 The computational grid used in this simulation, where the scalars are stored at the cell centers and the vector components are stored on the cell faces.

The energy equation is solved in an explicit fashion (Equation 2.43) and then corrected to satisfy the interface boundary condition (Equation 2.44).

$$T^* = \frac{(cT)^n}{c(\phi)^{n+1}} + \frac{\Delta t}{c(\phi)^{n+1}}\left(-\vec{V} \bullet \nabla\left(c(\phi)T\right)^n + \frac{\nabla \bullet (k(\phi)\nabla T)^n}{\rho(\phi)^n} \right) \tag{2.43}$$

$$T_{sat} = T_{i,j}^{n+1} - \phi_{i,j}\vec{n} \bullet \nabla T\Big|_{i,j}^{n+1} \qquad \text{if } [x_i, y_j] \text{ is next to the interface} \tag{2.44a}$$

$$T^{n+1} = T^* \qquad \text{else} \tag{2.44b}$$

The nodes next to the interface are determined by looking for a change in the sign of the level set field. A second-order essentially non-oscillatory scheme (ENO) [Chang et. al. (1996)] is used for the advective operator in the energy equation and the diffusion operator is approximated with second-order central differences. The temperature gradient in Equation (2.44a) is approximated using the forward and backward difference

operators, which is outlined in Section (2.6). The temperature field is second-order accurate in space and first-order accurate in time.

The level set advection equation is discretized explicitly where the time derivatives are approximated with a fourth-order Runge-Kutta method (4RK). The 4RK method can be written as a series of forward difference steps, which is shown below in Equation (2.45) corresponding to the advection equation.

$$\phi^{m+1} = \phi^{n} - \beta^{m}\Delta t\left(\vec{V}_{INT} \bullet \nabla\phi^{m}\right) \qquad \text{for } m=0\ldots3 \tag{2.45}$$

The coefficients for β^{m} are [1/4, 1/3, 1/2, 1]; likewise, *m=0* and *m=4* correspond to the *n* and *n+1* time levels respectively. The gradient of the level set field is approximated with a fifth-order weighted essentially non-oscillatory scheme (WENO) [Jiang and Peng (2000)]. Along the edges of the solution domain the gradient operator is approximated with either the second-order or first-order accurate essentially non-oscillatory schemes (ENO) depending on how close the node is to the boundary. The accuracy of the WENO scheme varies from third-order to fifth-order accurate depending on the smoothness of the field.

The time derivative in the level set reinitialization equation was also approximated with the fourth-order Runge-Kutta method previously discussed. The discrete form of the reinitialization equation is shown in Equation (2.46).

$$\phi^{m+1} = \phi^{n} - \beta^{m}\Delta t S(\phi_0)\left(\left\|\nabla\phi^{m}\right\|_2 - 1\right) \qquad \text{for } m=0\ldots3 \tag{2.46}$$

The coefficients are identical to the ones in Equation (2.40). The spatial derivatives in the two-norm of the gradient are approximated with a second-order ENO scheme suggested by Osher and Sethian (1988).

The time step restrictions corresponding to the time discretization techniques implemented in this study are given by Equations (2.47a) – (2.47f).

$$\Delta t_V^{\max} = \frac{1}{\left(\frac{u_{\max}}{\Delta x} + \frac{v_{\max}}{\Delta y} \right)} \tag{2.47a}$$

$$\Delta t_g^{\max} = \sqrt{\frac{\Delta_{\min}}{g}} \tag{2.47b}$$

$$\Delta t_\sigma^{\max} = \sqrt{\rho_{\min} \Delta_{\min}^3 \frac{3}{4\sigma}} \tag{2.47c}$$

$$\Delta t_\mu^{\max} = \frac{1}{2\left(\left(\frac{\mu}{\rho} \right)_{\max} \left(\frac{1}{\Delta x^2} + \frac{1}{\Delta y^2} \right) \right)} \tag{2.47d}$$

$$\Delta t_k^{\max} = \frac{1}{2\left(\left(\frac{k}{\rho c} \right)_{\max} \left(\frac{1}{\Delta x^2} + \frac{1}{\Delta y^2} \right) \right)} \tag{2.47e}$$

$$\Delta t_{V_{\text{int}}}^{\max} = \frac{1}{\frac{(u_{\max} + q_{\max})}{\Delta x} + \frac{(v_{\max} + q_{\max})}{\Delta y}} \tag{2.47f}$$

The time step used for the simulation was,

$$\Delta t = 0.8 * \min\left(\Delta t_V^{\max} + \Delta t_g^{\max} + \Delta t_\sigma^{\max} + \Delta t_\mu^{\max} + \Delta t_k^{\max} + \Delta t_{V_{INT}}^{\max} \right), \tag{2.48}$$

where $\Delta_\mu^{\max}$ or $\Delta_k^{\max}$ typically restricted the size of the time step.

2.9 Solution Strategy

The strategy for solving the governing equations is outlined below.

1. Calculate the projected velocity field, V^*, using Equation (2.40)
2. Calculate the new level set field using Equation (2.45)
    a. Reinitialize the level set field to be a signed distance function from the interface by solving Equation (2.46)
    b. Construct the new smeared Heaviside function by solving Equation (2.18), and also store the Heaviside function at the previous time level.
3. Calculate the new temperature field by solving Equation (2.43)
    a. Apply the interface temperature condition using Equation (2.44a)
4. Construct the new ghost node values using Equation (2.38)
5. Evaluate the continuity equation source term using Equation (2.14)
6. Calculate the new pressure field using Equation (2.42)
7. Calculate the new velocity field using Equation (2.41)
8. Now, go back to step one

2.10 Numerical Tests

Two numerical tests were preformed to verify the suggested liquid-vapor phase transition method works. The first test problem was a one dimensional phase-change problem that Son and Dhir (1998), and Welch and Wilson (2000) used to evaluate their

phase-change schemes (Figure 2.11). The second test problem was a modification of the two dimensional phase-change problem that Juric and Tryggvason (1996) and Udaykumar et. al. (1999) used to evaluate their solidification schemes (Figure 2.11).

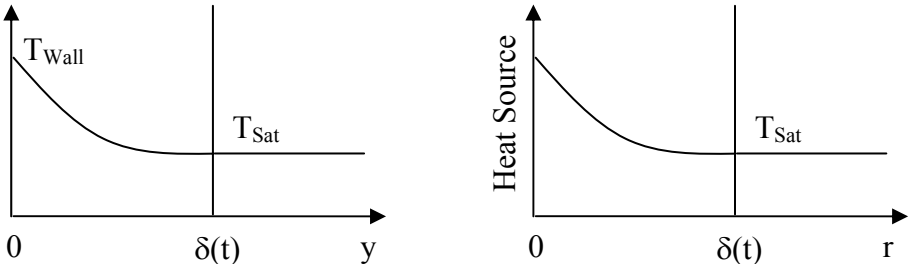

Figure 2.11 The liquid-vapor phase-change test problems - the left plot corresponds to the one-dimensional numerical test, and the right plot corresponds to the two-dimensional numerical test.

2.10.1 One-Dimensional Test

The energy equation for the one-dimensional test problem in the vapor phase is given by,

$$\frac{\partial T_v}{\partial t} = \alpha_v \frac{\partial^2 T_v}{\partial x^2} \tag{2.49}$$

where the boundary conditions are,

$$T_v(x = \delta(t), t) = T_{sat} \tag{2.50a}$$

$$T_v(x = 0, t) = T_{wall}\,. \tag{2.50b}$$

Likewise, the energy jump condition on the interface is,

$$\rho_v h_{fg} \frac{d\delta}{dt} = -k_v \left.\frac{\partial T_v}{\partial x}\right|_{x=\delta(t)} \tag{2.51}$$

where, δ is the interface position. The temperature in the liquid phase is maintained at T_{sat}, and the temperature in the vapor phase is given by Equation (2.51). The analytical solution for the position of the interface is given by,

$$\delta(t) = 2\lambda\sqrt{\alpha_v t} \tag{2.52}$$

where λ is solution of the transcendental equation below,

$$\lambda e^{\lambda^2} erf(\lambda) = \frac{c_{p_v}(T_{wall} - T_{sat})}{h_{fg}\sqrt{\pi}}. \tag{2.53}$$

Likewise, the analytical solution for the temperature is given by,

$$\frac{T_v(x,t) - T_{Wall}}{T_{SAT} - T_{Wall}} = \frac{erf\left(\frac{y}{\sqrt{4\alpha_v t}}\right)}{erf(\lambda)}. \tag{2.54}$$

For additional information on the analytical solution see Özişik (1992).

The analytical solution for the one-dimensional test problem at 1 second was used as the initial condition for the numerical solution and then results were compared at 2, 3, 4, and 5 seconds on 40x40, 60x60, 70x70, 80x80, and 90x90 grids. The properties for the test problem correspond to a Jacob number of 9, $Ja = c_v(T_{Wall}-T_{Sat})/h_{fg}$, and a thermal diffusivity of 10^{-3} m^2/s in the vapor phase; in addition, the solution domain was 1m by 1m. The error norm used for evaluating the performance of the scheme is shown by Equation (2.55) and it corresponds to the same error norm used by Udaykumar (1999).

$$L_2 = \sqrt{\frac{\sum_{i,j}\left(T_{i,j} - T_{Exact}\right)^2}{N_x N_y}} \tag{2.55}$$

Figure (2.12) shows the numerical calculation of the interface location along with the analytical solution corresponding to a 90x90 grid. The suggested phase change

scheme was able to solve the one-dimensional phase transition problem with reasonable accuracy. The L_2 error norm corresponding to the interface location is shown in Figure (2.13) as a function of the grid size. The numerator in the L_2 error norm was modified to account for the comparison of a single value. The modified numerator was the square of the error between the numerically calculated interface position and the analytical value. The L_2 error norm plot (Figure 2.14) illustrates that the phase-change method is second-order accurate.

The error in the temperature field was also second-order accurate. Figure (2.15) shows the L_2 error norm for the temperature field corresponding to the one-dimensional test. It is important for the phase-change method to maintain the second-order accuracy of the temperature field.

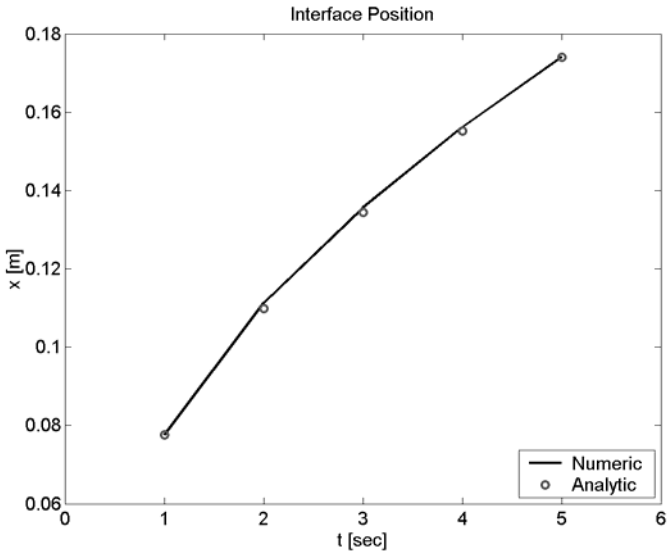

Figure 2.12 The interface position determined analytically and numerically using a 90x90 grid.

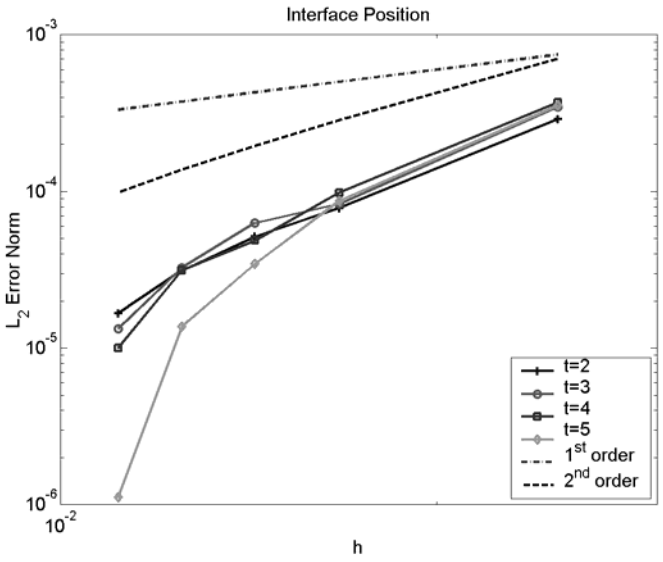

Figure 2.13 The L_2 error norm for the interface position as a function of the grid size, h, for the one-dimensional test problem

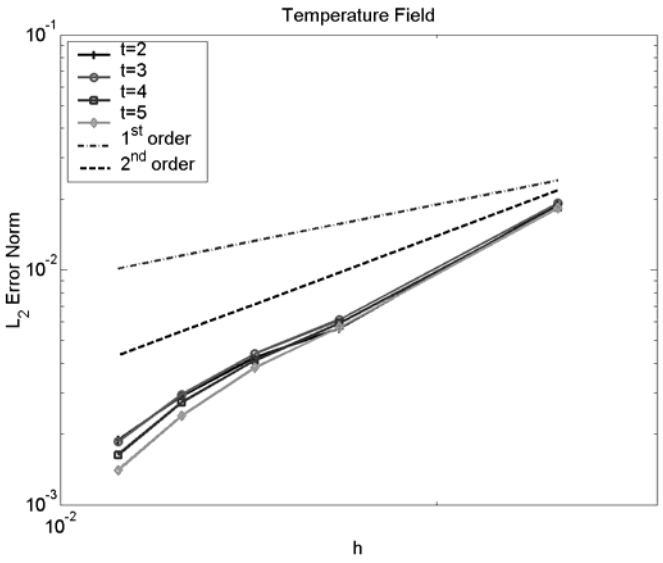

Figure 2.14 The L_2 error norm for the temperature as a function of the grid size, h, for the one-dimensional test problem

2.10.2 Two-Dimensional Test

The two-dimensional test problem is very similar to the one-dimensional test problem. The energy equation in the vapor phase is given by,

$$\frac{\partial T_v}{\partial t} = \alpha_v \frac{1}{r}\frac{\partial}{\partial r}\left(\frac{\partial T_v}{\partial r}\right) \tag{2.56}$$

where the boundary conditions are,

$$T_v(x = \delta(t), t) = T_{sat} \tag{2.57a}$$

$$\lim_{r\to 0}\left(2\pi k_v \frac{\partial T_v}{\partial r}\right) = Q\,. \tag{2.57b}$$

Likewise, the liquid-phase temperature is always at T_{sat}. The interface jump condition is given by Equation (2.58).

$$\rho_v h_{fg}\frac{d\delta}{dt} = -k_v \left.\frac{\partial T_v}{\partial r}\right|_{x=\delta(t)} \tag{2.58}$$

The analytical solution for the temperature in the vapor phase is,

$$T_v(r,t) = T_{SAT} + \frac{Q}{4\pi k_v}\left(E_1\left(\frac{r^2}{4\alpha_v t}\right) - E_1\left(\lambda^2\right)\right) \tag{2.59}$$

where E_1 is the exponential integral function given by Equation (2.60), and λ is the solution of the transcendental equation shown by Equation (2.61).

$$E_1(a) = \int_1^\infty \frac{e^{-au}}{u}du \tag{2.60}$$

$$\lambda^2 \alpha_v \rho h_{fg} = \frac{Q}{4\pi}e^{-\lambda^2}\,. \tag{2.61}$$

The radius of the interface is given by,

$$\delta(t) = 2\lambda\sqrt{\alpha_v t} \tag{2.62}$$

Özişik (1992) gives an in-depth discussion of analytical solutions for radial phase-change problems.

The two-dimensional test problem used the same properties as the one-dimensional test and a heat source of $1W/m^3$; in addition, the analytical solution at 1 second was also used as the initial condition for the numerical solution. To handle the heat source, the exact temperature was applied to the nodes near the source for every time step; this follows the work of both Juric and Tryggvason (1996), and Udaykumar et. al. (1999). The exact interface radius was slightly larger than 0.08m at 1 second so forcing the nodes near the source to be the exact temperature should not produce erroneous error results. Figure (2.15) shows the numerical results for the interface location at 2 and 3 seconds for a 90x90 grid along with the analytical solution. The L_2 error norm for the position of the interface as a function of the grid size is shown in Figure (2.16), and the method maintained the second-order accuracy in multiple dimensions.

The errors in the temperature field were slightly larger in the two-dimensional test problem than the one-dimensional test problem; however, the temperature field was still second-order accurate. The L_2 error norm for the temperature field is shown in Figure (2.17). In multiple dimensions the phase change scheme worked extremely well and was able to properly maintain the curvature of the interface and the temperature field with second-order accuracy.

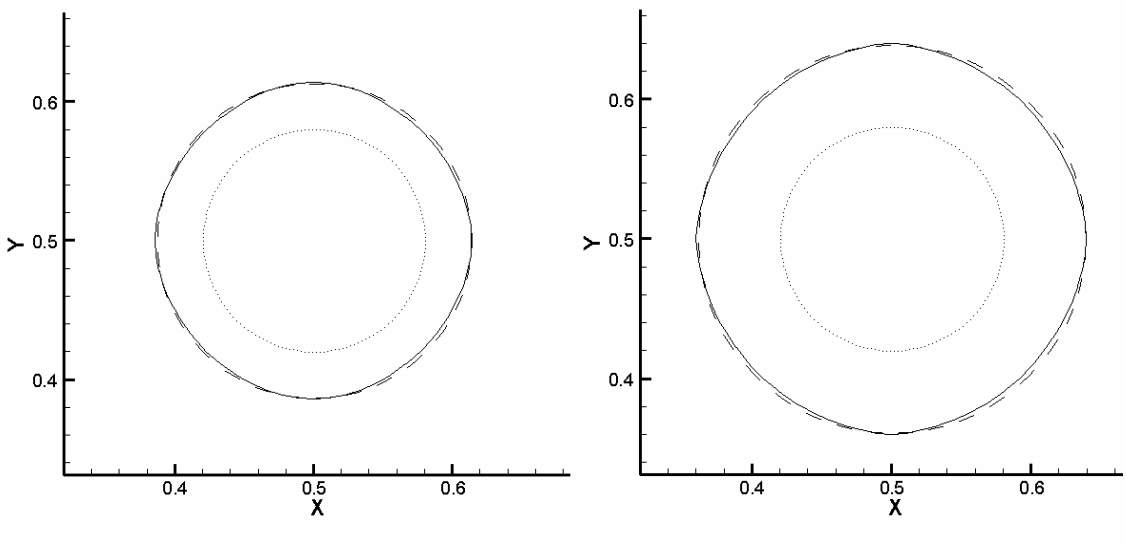

Figure 2.15 **The interface location at 2 seconds is shown on the top and the interface location at 3 seconds is shown on the bottom for a 90x90 grid; the dotted line corresponds to the initial position, the solid line corresponds to the numerical solution at the respective time, and the dashed line corresponds to the analytical solution at the respective time.**

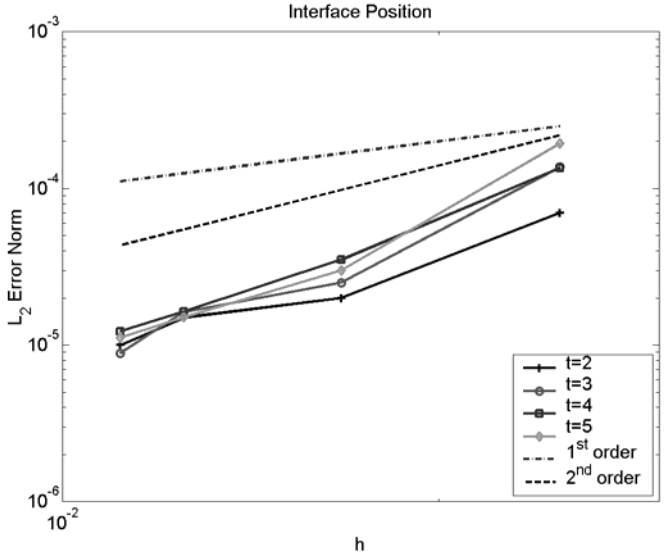

Figure 2.16 **The L_2 error norm for the interface position as a function of the grid size, h, for the two-dimensional test problem**

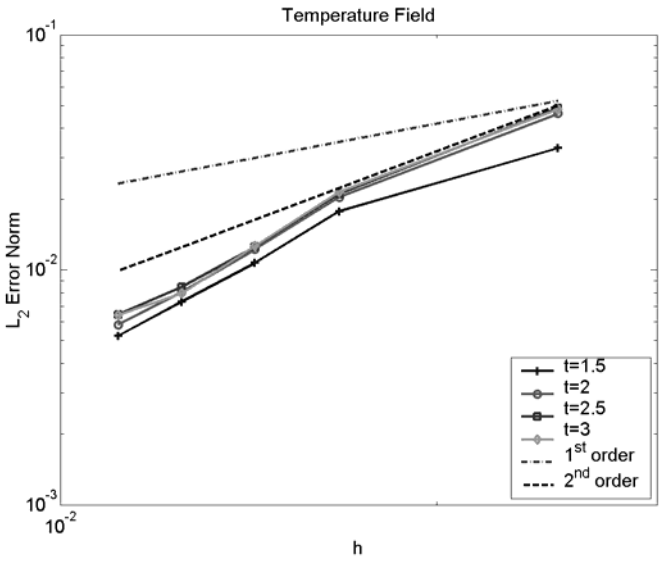

Figure 2.17 The L_2 error norm for the temperature as a function of the grid size, h, for the two-dimensional test problem

2.11 Film Boiling Simulations

A film boiling simulation was performed to test the performance of the new phase transition method. The width of the simulation corresponds to the critical Taylor wavelength, λ, (Equation 2.63) and the height of the simulation was 2 times the critical Taylor wavelength.

$$\lambda = 2\pi\left(\frac{3\sigma}{(\rho_l - \rho_v)g}\right)^{1/2}. \tag{2.63}$$

The material properties used in the first simulation are shown in Table (2.1). The bottom wall was maintained at a temperature 9 °Celsius above the saturation temperature, the side walls were insulated (symmetric boundary conditions), and the top wall was maintained at the saturation temperature. The top boundary was a pressure

condition, the sides were symmetric boundaries, and the bottom wall was a slip conditions. The initial condition was a vapor layer on the bottom wall (Equation 2.64a) that was perturb in the center (Equation 2.64b) such that the plume would be in the center.

$$\phi = -d + y \qquad \text{(if } \phi < 0.3\lambda \text{ or } \phi > 0.7\lambda \text{)} \qquad (2.64a)$$

$$\phi = \sqrt{\left(x - \frac{\lambda}{2}\right)^2 + (y + 2d)^2} - (3d + 2\Delta y) \qquad \text{else} \qquad (2.64b)$$

The constant, d, was chosen to be 0.019 for the film boiling simulations, and Equation (2.57b) perturbed the interface by $2\Delta y$. Equations (2.64a) and (2.64b) are a signed distance function from the interface except where the two equations merge, so the numerical technique suggested by Sussman (1994) (Equation 2.24) was used to make the entire field a signed distance function from the interface. The results from the first film boiling simulation are shown in Figure (2.18).

Table 2.1 Properties used with the film boiling simulations

Density [kg/m^3]	Viscosity [kg/sm]	Specific Heat [J/kgK]	Thermal Conductivity [W/mK]	Surface Tension [N/m]	Enthalpy of Vaporization [J/kgK]
$\rho_l = 100$	$\mu_l = 0.024$	$c_l = 8.0$	$k_l = 0.02$	$\sigma = 0.1$	$h_{fg} = 50$
$\rho_v = 1$	$\mu_v = 0.012$	$c_v = 2.0$	$k_v = 0.01$		

To test the performance the new phase transition method, the heat transfer coefficient was compared with the Berrenson correlation. The heat transfer coefficient,

h_c, is the proportionality constant relating the temperature difference to the heat flux (Equation 2.65).

$$h_c = \frac{-k_v \left.\frac{\partial T}{\partial y}\right|_{Wall}}{\Delta T_{SAT}} \tag{2.65}$$

The wall super heat, ΔT_{SAT}, is equal to $T_{Wall} - T_{SAT}$. The heat transfer coefficient for the film boiling simulation is shown in Figure (2.19) along with the Berrenson correlation, which is shown by Equation (2.66) [Collier and Thome (1996)]. The film boiling simulation was performed on a two-dimensional Cartesian grid so the results were multiplied by $\pi/4$ to account for an axisymmetric bubble. The results from the film boiling simulation are in good agreement with the Berrenson correlation.

$$h_c = 0.425\left[\frac{g(\rho_l - \rho_v)\rho_v k_v^3 h'_{fg}}{\mu_v \Delta T_{SAT}\left(\frac{\sigma}{g(\rho_l - \rho_v)}\right)^{1/2}}\right]^{1/4} \tag{2.66a}$$

$$h'_{fg} = h_{fg}\left(1 + 0.68\left(\frac{c_v \Delta T_{SAT}}{h_{fg}}\right)\right) \tag{2.66b}$$

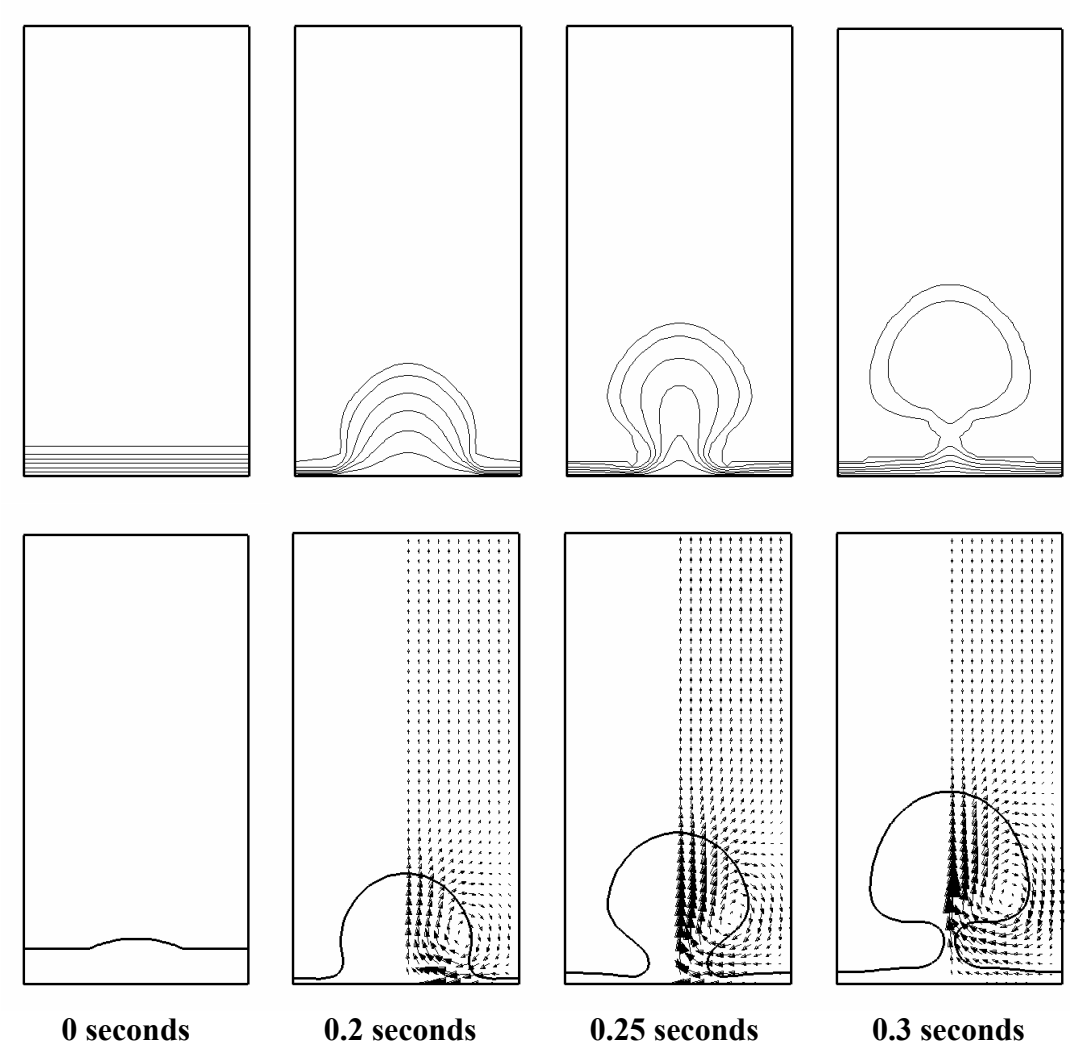

Figure 2.18 Film boiling simulation results at 0, 0.2, 0.25, and 0.3 seconds respectively, where the top row shows the temperature contours, and the bottom row shows the interface location and velocity field.

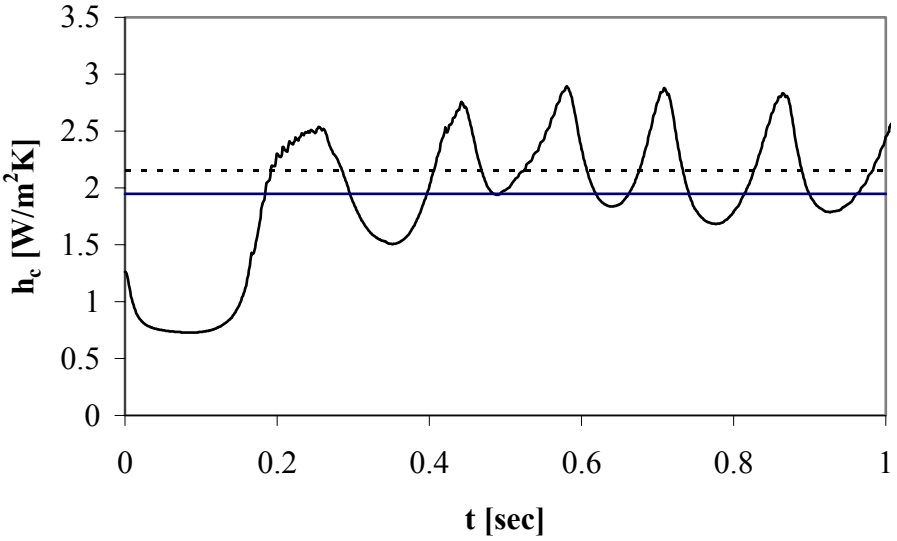

Figure 2.19 The heat transfer coefficient calculated by the Berrenson correlation (solid horizontal line) and calculated numerically, where the dashed horizontal line is the average of the numerical results after the first bubble departs.

A subcooled boiling simulation was performed to test the ability to maintain the interface at the saturation temperature. The properties were the same as the saturated film boiling test. The temperature on the bottom wall was 9 °C above the saturation temperature, and the ambient fluid was 1 °C below the saturation temperature. The top was maintained at the ambient temperature and the sides were insulated. The fluid boundary condition on the top corresponds to a pressure boundary, and slip boundary conditions were on the other sides. The initial condition for the film boiling simulation was the same as the previous test. The results from the second film boiling simulation are shown at 0.0, 0.25, 0.30, and 0.35 seconds in Figure (2.20). The phase change scheme maintained the interface at the saturation temperature; moreover, the method preserved the steep temperature profile near the heated wall.

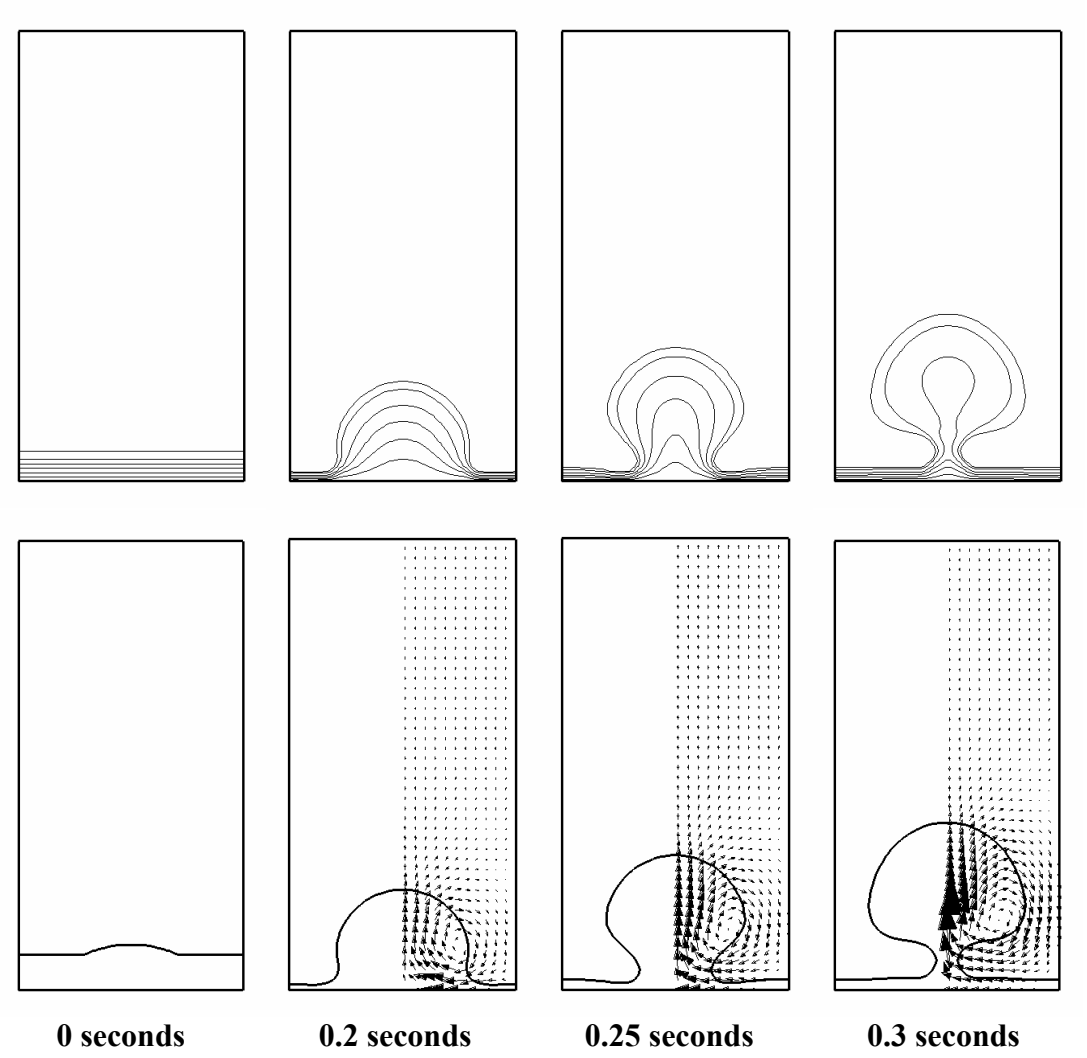

Figure 2.20 **Film boiling simulation results at 0, 0.20, 0.25, and 0.3 seconds respectively, where the top row shows the temperature contours, and the bottom row shows the interface location and velocity field.**

CHAPTER 3
IMPROVEMENTS TO THE LEVEL SET METHOD

3.1 Overview

The level set method is a great tool for simulating multiphase flows; however, it has the tendency to artificially move the interface, which causes losses or gains of volume. Several techniques have been proposed for fixing the volume loss or gain problem. The first technique studied is the coupled level set volume of fluid (CLSVOF) method [Sussman and Pucket (2000), and Son (2003)]. The VOF scheme used with the CLSVOF method is referred to as the PLIC (Piecewise linear calculation) VOF method [Youngs (1984), Rider and Kothe (1998)], because it represents the interface as a piecewise linear function. The level set method and the VOF method are coupled by reinitializing the level set field to be a signed distance function from the piecewise linear interface; as a result, the zero contour of the level set field satisfies the volume fraction field. The CLSVOF method studied in this work implements the standard reinitialization technique [Sussman (1994)] to maintain the level set field as a signed distance function from the interface.

The second technique studied involves solving an initial value problem to force volume conservation when reinitializing the level set field to be a signed distance function from the interface. Chang et. al. (1996) suggested solving an equation that shifts the interface to satisfy global volume conservation; likewise, Son (2001) extended the idea to account for multiple interfaces and phase transition. In this work, the initial

value techniques are compared with the CLSVOF method. In addition, a new initial value technique is discussed.

The purpose of this study is to investigate and present techniques for improving the accuracy of the level set method. The results from the CLSVOF method are compared to the standard level set method based on second-order ENO advection and fifth-order WENO advection respectively. Several advection tests are studied in this work along with two physical simulations. The first physical simulation is a droplet impacting a shallow pool, and the second simulation is film boiling. The CLSVOF method is modified to incorporate the phase transition technique discussed in the previous chapter. The results from this work will greatly improve the accuracy of multiphase simulations, including flows with phase transition.

3.2 The PLIC Volume of Fluid Method

The idea behind the volume of fluid method is to advect the volume fraction field and then reconstruct the interface using the volume fraction field. The volume fraction, F, is advected on an Eulerian mesh using Equation (3.1) where the velocity field, $\vec{V}$, is divergent free.

$$\frac{\partial F}{\partial t} + \vec{V} \bullet \nabla F = 0 \tag{3.1}$$

The properties of a cell can be represented as,

$$\gamma = \gamma_l F + \gamma_v (1 - F) \tag{3.2}$$

where γ_l and γ_v correspond to the properties of the respective phases such as density, specific heat, etc. The liquid properties correspond to a volume fraction of 1, and the vapor properties correspond to a volume fraction of 0. The volume fraction advection equation can be written in terms of the volume fraction fluxes (Equation 3.3) and directionally split (Equation 3.4) [Puckett et. al. (1997)].

$$\frac{\partial F}{\partial t} + \frac{\partial (Fu)}{\partial x} + \frac{\partial (Fv)}{\partial y} = F \nabla \bullet \vec{V} \tag{3.3}$$

$$\frac{\widetilde{F} - F^n}{\Delta t} + \frac{\partial (F^n u^n)}{\partial x} = \widetilde{F} \frac{\partial u^n}{\partial x} \tag{3.4a}$$

$$\frac{F^{n+1} - \widetilde{F}}{\Delta t} + \frac{\partial (\widetilde{F} v^n)}{\partial y} = \widetilde{F} \frac{\partial v^n}{\partial y} \tag{3.4b}$$

The directionally split algorithm alternates directions to prevent any biasing. The volume fraction on right hand side of Equation (3.4a) is discretized implicitly time, where the right hand side of Equation (3.4b) is discretized explicitly in time. The fluxes in Equation (3.4) are constructed by measuring the exact amount of material leaving the cell, which prevents numerical diffusion and maintains a sharp interface. The flux construction process requires knowledge of the interface location and orientation; so after each directional step, the interface is reconstructed to satisfy the volume fraction.

The volume of fluid method can also be used for non-divergent free velocity fields. For this type of problem the density, ρ, is advected on an Eulerian mesh instead of the volume fraction (Equation 3.5).

$$\frac{\partial \rho}{\partial t} + \nabla \bullet (\rho \vec{V}) = 0 \tag{3.5}$$

The concept for constructing fluxes is identical to procedure outlined above. The density fluxes are constructed using the interface location and orientation such that the exact

amount of material leaves the cell. Then the interface is reconstructed such that it satisfies the correct volume fraction, where the volume fraction is given by Equation (3.6).

$$F = \frac{\rho - \rho_v}{\rho_l - \rho_v} \tag{3.6}$$

The challenge with using the PLIC volume of fluid methodology is properly representing the interface with piecewise linear lines. Once the interface is known in each cell the technique is trivial. There are multiple techniques suggested for reconstructing the interface, where one of the newest techniques is the coupled level set volume of fluid (CLSVOF) method.

3.3 The Coupled Level Set Volume of Fluid (CLSVOF) Method

The CLSVOF method is based on the PLIC volume of fluid method, which was initially proposed by Youngs (1984). The CLSVOF method takes advantage of the level set field to (1) construct the interface, and (2) improve the accuracy of the interface geometry. The interface reconstruction process requires the normal vector, which can be found easily with the smooth level set field. Likewise, the curvature can be found by using the smooth level set field. The CLSVOF concept is to advect both the level set field and the volume fraction field (Equation 2.13 and Equation 3.1), and then reinitialize the level set field to be a signed distance function from the reconstructed interface.

3.3.1 Advection for Incompressible Flows

Following the work of Puckett et. al. (1997), and Sussman and Puckett (2000) the advection equation is written,

$$\frac{\partial s}{\partial t} + \nabla \bullet (\vec{V}s) = s\nabla \bullet \vec{V} \,. \tag{3.7}$$

where s is a scalar quantity. The idea is to directionally split the advection equation and alternate the directions to prevent any biasing.

$$\frac{\partial s}{\partial t} + \frac{\partial us}{\partial x} = s\frac{\partial u}{\partial x} \tag{3.8a}$$

$$\frac{\partial s}{\partial t} + \frac{\partial vs}{\partial y} = s\frac{\partial v}{\partial y} \tag{3.8b}$$

The scalar variable, s is discretized implicitly on the right hand side of Equations (3.8a), and explicitly on the right hand side of Equation (3.8b), which maintains the conservation of s. An operator split algorithm for advecting a scalar quantity, s, is then given by Equation (3.9),

$$\widetilde{s}_{i,j} = \frac{s^{n}_{i,j,k} + (\Delta t / \Delta x)\left(G_{i-1/2,j} - G_{i+1/2,j}\right)}{1 - (\Delta t / \Delta x)\left(u_{i+1/2,j} - u_{i-1/2,j}\right)} \tag{3.9a}$$

$$s^{n+1}_{i,j} = \widetilde{s}_{i,j} + \frac{\Delta t}{\Delta y}\left(\widetilde{G}_{i,j-1/2} - \widetilde{G}_{i,j+1/2}\right) + \widetilde{s}_{i,j}\,\frac{\Delta t}{\Delta y}\left(v_{i,j+1/2} - v_{i,j-1/2}\right) \tag{3.9b}$$

where $G_{i+1/2,j} = s_{i+1/2,j}u_{i+1/2,j}$, $G_{i,j+1/2} = s_{i,j+1/2}u_{i,j+1/2}$, $\widetilde{G}_{i+1/2,j} = \widetilde{s}_{i+1/2,j}u_{i+1/2,j}$, and $\widetilde{G}_{i,j+1/2} = \widetilde{s}_{i,j+1/2}u_{i,j+1/2}$. The algorithm shown by Equation (3.9) has been shown to produce second-order accurate results [Puckett et. al. (1997)].

When the scalar variable corresponds to the volume fraction, F, then the flux, $G_{i+1/2}$, corresponds to the volume fraction at the east face times the velocity; likewise, the flux entering the cell, $G_{i-1/2}$ corresponds to the volume fraction at the west face times the velocity. If the velocity in the x-direction is positive, then the volume fraction at the east face is the volume fraction that is leaving the $(i,j)^{th}$ cell; likewise, the volume fraction at the west face is the volume fraction that is leaving the $(i-1,j)^{th}$ cell. The volume fraction leaving a cell is found by calculating the region of material, Ω, that is leaving the cell, ($\Delta\alpha$, $\Delta\beta$). The volume fraction of a region can be expressed in terms of the sharp Heaviside function, $\overline{H}$ (Equation 3.10).

$$F = \frac{1}{\Delta\alpha\Delta\beta}\iint_{\Omega}\overline{H}(\overline{\phi})dA \tag{3.10}$$

The sharp Heaviside function, $\overline{H}$, is constructed from the piecewise linear interface, which corresponds to a linearization of the level set field, $\overline{\phi}(x,y)$. The integral in Equation (3.10) is evaluated geometrically using analytical expressions. Figure (3.2) shows an example of how the volume fraction flux leaving the cell is calculated in the x-direction. In Figure (3.2), the flux $G_{i+1/2}$ leaving the cell corresponds to,

$$\alpha \in \left[x_{i+1/2} - udt, x_{i+1/2}\right] \tag{3.11a}$$

$$\beta \in \left[y_{j-1/2}, y_{j+1/2}\right]. \tag{3.11b}$$

If $u_{i+1/2}<0$ on the east face, then the region would be,

$$\alpha \in \left[x_{i+1/2}, x_{i+1/2} - udt\right] \tag{3.12a}$$

$$\beta \in \left[y_{j-1/2}, y_{j+1/2}\right]. \tag{3.13b}$$

and the sharp Heaviside function in Equation (3.10) would correspond to the east cell.

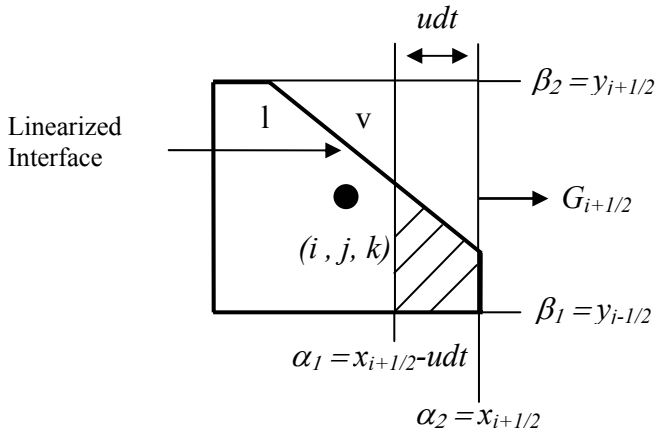

Figure 3.1 The volume fraction flux, $G_{i+1/2}$, leaving the cell corresponds to the region, $\Delta\alpha\Delta\beta$, where the integral of the Heaviside function over the exit region corresponds to the shaded area. The letters l and v correspond to the liquid and vapor phases respectively.

It is possible to generate volume fractions greater than 1 and less then zero, with a directionally split advection algorithm. Therefore, after each advection step the volume fraction field is clipped to keep it in the range of 0 and 1. The level set field is used as an indicator field to assist in the clipping process. If $|\phi| \geq 3/2\Delta$, then the volume fraction of the cell is 0 if $\phi<0$, or 1 if $\phi>0$.

When the scalar quantity, s, corresponds to the level set function, ϕ, then the flux, $G_{i+1/2}$, is merely the velocity on the face times the level set function value on the face. A second-order method can be easily used to construct the fluxes on the cell edges. Following the work of Sussman and Puckett (2000), the scalar values on the face are extrapolated in both space and time.

$$s_{i+\frac{1}{2},j,l} \approx s_{i,j,k} + \frac{\Delta x}{2}\frac{\partial s}{\partial x}\bigg|_{i,j,k} + \frac{\Delta t}{2}\frac{\partial s}{\partial t}\bigg|_{i,j,k} \quad \text{if} \quad u_{i+\frac{1}{2},j,k} > 0 \tag{3.14}$$

The advection scheme is directionally split so the time derivative is equal to,

$$\frac{\partial s}{\partial t} = -u\frac{\partial s}{\partial x}. \tag{3.15}$$

Approximating the spatial derivatives with central differences and substituting Equation (3.14) into (3.15) produces a second-order accurate technique for extrapolating the face values from the cell center data. The *x*-direction, *y*-direction, and *z*-direction formulations are shown by Equations (3.16) and (3.17) respectively.

$$s_{i+\frac{1}{2},j} = \begin{cases} s_{i,j} + \dfrac{\Delta x}{2}\left(1 - u_{i+\frac{1}{2},j}\dfrac{\Delta t}{\Delta x}\right)\dfrac{s_{i+1,j} - s_{i-1,j}}{\Delta x} & if \quad u_{i+\frac{1}{2},j} > 0 \\ s_{i+1,j} - \dfrac{\Delta x}{2}\left(1 + u_{i+\frac{1}{2},j}\dfrac{\Delta t}{\Delta x}\right)\dfrac{s_{i+2,j} - s_{i,j}}{\Delta x} & if \quad u_{i+\frac{1}{2},j} < 0 \end{cases} \tag{3.16}$$

$$\widetilde{s}_{i,j+\frac{1}{2}} = \begin{cases} \widetilde{s}_{i,j} + \dfrac{\Delta y}{2}\left(1 - v_{i,j+\frac{1}{2}}\dfrac{\Delta t}{\Delta y}\right)\dfrac{\widetilde{s}_{i,j+1} - \widetilde{s}_{i,j-1}}{\Delta y} & if \quad v_{i,j+\frac{1}{2}} > 0 \\ \widetilde{s}_{i,j+1} - \dfrac{\Delta y}{2}\left(1 + v_{i,j+\frac{1}{2}}\dfrac{\Delta t}{\Delta y}\right)\dfrac{\widetilde{s}_{i,j+2} - \widetilde{s}_{i,j}}{\Delta y} & if \quad v_{i,j+\frac{1}{2}} > 0 \end{cases} \tag{3.17}$$

The first-order donor cell technique just uses the center values of the respective cell and does not have the extra terms on the right side of Equations (3.16) and (3.17).

The level set function is advected using the directionally split method, because it is used to reconstruct the interface for the next directional advection step. During the advection process, the zero contour of the level set function will move from artificial diffusion, which causes losses or gains in volume. To fix this problem the VOF method is used to shift the interface back to the correct orientation that satisfies mass conservation. The level set field is reinitialized to satisfy the volume fractions after each advection step in the respective directions to prevent any loss of mass.

3.3.2 Advection for Flows with Phase Change

If the flow is not divergent free, then the advection equation in discrete form for a scalar value, s, is

$$\frac{s^{n+1}-s^{n}}{\Delta t}+\frac{G_{i+1/2,j}-G_{i-1/2,j}}{\Delta x}+\frac{G_{i,j+1/2}-G_{i,j-1/2}}{\Delta y}=0 \tag{3.18}$$

where G is the scalar flux. A directionally split form of the advection equation is,

$$\frac{\widetilde{s}-s^{n}}{\Delta t}+\frac{G_{i+1/2,j}-G_{i-1/2,j}}{\Delta x}=0 \tag{3.19a}$$

$$\frac{s^{n+1}-\widetilde{s}}{\Delta t}+\frac{\widetilde{G}_{i,j+1/2}-\widetilde{G}_{i,j-1/2}}{\Delta y}=0 \tag{3.19b}$$

where the fluxes at the fractional time level, $\widetilde{G}$ corresponds to the velocity at the n^{th} time level times the scalar value at the fractional time level, $\widetilde{s}$.

When the scalar variable corresponds to the density, ρ, then the flux, G, corresponds to the density leaving the cell times the velocity. The density leaving a cell is found by calculating the region of material, Ω, that is leaving the cell, ($\Delta\alpha$, $\Delta\beta$); then, the volume of each phase in the exit region is used to calculate the density on the face. The density of a region can be expressed in terms of the sharp Heaviside function, $\overline{H}$ (Equation 2.20).

$$\rho=\rho_{v}+(\rho_{l}-\rho_{v})F=\rho_{v}+(\rho_{l}-\rho_{v})\frac{1}{\Delta\alpha\Delta\beta}\iint_{\Omega}\overline{H}(\bar{\phi})dA \tag{3.20}$$

The sharp Heaviside function, $\overline{H}$, is constructed from the piecewise linear interface, and the integral is calculated geometrically.

It is possible to generate a density in a cell that corresponds to a volume fraction that is greater than 1 or less then 0, with a directionally split advection algorithm. To fix this problem, the volume fractions are calculated after each advection step and then clipped to keep the volume fractions in the range of 0 and 1. After the volume fractions are clipped, the new density is calculated. The clipping process is only carried out on the nodes that are greater than 3/2Δ from the interface.

When the scalar quantity, s, corresponds to the level set function, ϕ, then the flux, $G_{i+1/2}$, is merely the interface velocity on the face times the level set value on the face. The interface velocity is given by Equation (2.8); likewise, the value on the face is constructed according to the first-order donor cell technique.

3.3.3 Calculating Volume Fractions

The volume fraction, F is given by,

$$F = \frac{1}{\Delta x \Delta y \Delta z} \iiint_{\Omega} \overline{H}(\overline{\phi}(x,y,z))dV \tag{3.21}$$

where Ω is the domain of the cell. The sharp Heaviside function in Equation (3.21) is constructed from a linearization of the level set field, $\overline{\phi}(x,y,z)$, which is shown by Equation (3.22).

$$\overline{\phi}(x,y,z) = \phi_{i,j,k} + (x - x_i)\frac{\partial \phi}{\partial x}\bigg|_{i,j,k} + (y - y_j)\frac{\partial \phi}{\partial y}\bigg|_{i,j,k} + (z - z_j)\frac{\partial \phi}{\partial z}\bigg|_{i,j,k} + O(h^2) \tag{3.22}$$

The integral of the sharp Heaviside function is calculated by finding the area of the polygon that is formed by the interface cutting though the cell if it is a two-dimensional problem, or the volume of the polyhedron if it is a three-dimensional problem. Likewise, the interface corresponds to $\overline{\phi} = 0$. Son (2003) derived analytical expressions for the area of a polygon, and the volume of a polyhedron. Using these expressions, the volume fraction of a polygon region is,

$$F = \frac{\frac{1}{2}\left[\Delta x_0 \Delta y_0 - \frac{\Delta y_0}{\Delta x_0}\max(\Delta x_0 - \Delta x, 0)^2 - \frac{\Delta x_0}{\Delta y_0}\max(\Delta x_0 - \Delta y, 0)^2\right]}{\Delta x \Delta y} \tag{3.23}$$

and the volume fraction of a polyhedron is,

$$\begin{aligned} F = \frac{1}{6}\Bigg[& \Delta x_0 \Delta y_0 \Delta z_0 - \frac{\Delta y_0 \Delta z_0}{\Delta x_0^2}\max(\Delta x_0 - \Delta x, 0)^3 + \\ & - \frac{\Delta x_0 \Delta z_0}{\Delta y_0^2}\max(\Delta y_0 - \Delta y, 0)^3 - \frac{\Delta x_0 \Delta y_0}{\Delta z_0^2}\max(\Delta z_0 - \Delta z, 0)^3 + \\ & + \frac{\Delta x_0 \Delta z_0}{\Delta y_0^2}\max(\Delta y_0 - \Delta y - \frac{\Delta y_0}{\Delta z_0}\Delta z, 0)^3 \Bigg] \frac{1}{\Delta x \Delta y \Delta z} \end{aligned} \tag{3.24}$$

where Δx_0 is the distance to the x-intercept of the interface, Δy_0 is the distance to the y-intercept of the interface, and Δz_0 is the distance to the z-intercept of the interface (Figure 3.2).

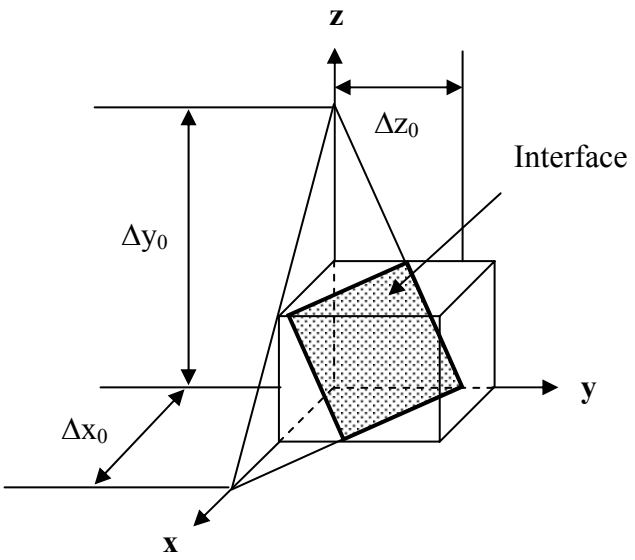

Figure 3.2 A diagram illustrating the x-intercept, y-intercept, and z-intercept locations for the interface where the dimensions of the box are *Δx* by *Δy* by *Δz*.

Equation (3.25) is another expression that can be used for calculating the area enclosed by a polygon.

$$A_{polygon} = \frac{1}{2}\sum_{v=1}^{n}(x_v y_{v+1} - x_{v+1} y_v) \tag{3.25}$$

The vertex coordinates of the polygon in Equation (3.25) are numbered in a clockwise fashion, where the $n+1$ vertex is the first vertex, $v=1$ (Figure 3.3).

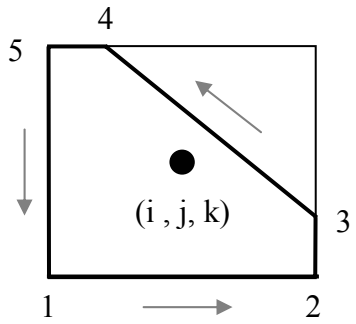

Figure 3.3 **A diagram illustrating the integration path for finding the area enclosed by a polygon, where the numbers correspond to the vertexes; the dimensions of the box are Δx by Δy.**

3.3.4 Reconstructing the Interface

The interface must be reconstructed after each directional-advection step such that it satisfies the volume fraction. In the PLIC VOF method, the interface in each cell can be represented by a line equation,

$$\vec{n} \bullet \vec{r} + c = 0 \tag{3.26}$$

where $\vec{n}$ is the normal vector of the interface and $\vec{r}$ is a position vector to a point on the interface and c is a constant [Rider and Kothe (1997)]. Likewise, an indicator function can be formulated that indicates on which side of the interface a point is located.

$$I = \vec{n} \bullet \vec{r} + c \tag{3.27}$$

The normal vector points outward so when $I>0$ it is outside the interface, likewise, when $I<0$ it is inside the interface. The constant c must be found that corresponds to the correct volume fraction based on the normal vector. There are multiple techniques for determining the normal vector from the volume fraction field such that Equation (3.26)

has a unique solution [Rider and Kothe (1997)]. Equation (3.26) is a simple linear equation that has the form,

$$A + (x_{Int} - x_i)B + (y_{Int} - y_j)C + (z_{Int} - z_j)D = 0 \tag{3.28}$$

which is nothing more than a linearization of the level set field evaluated along the interface (Equation 3.22). This is the power of the CLSVOF method, because it is not necessary to determine the normal vector from the volume fraction field; instead, the level set method can be used to calculate the normal vector. It is clear that the VOF method can be easily coupled with the level set field when reconstructing the interface.

$$A_{i,j,k} + (x_{Int} - x_i)\left.\frac{\partial \phi}{\partial x}\right|_{i,j,k} + (y_{Int} - y_j)\left.\frac{\partial \phi}{\partial y}\right|_{i,j,k} + (z_{Int} - z_j)\left.\frac{\partial \phi}{\partial z}\right|_{i,j,k} = 0 \tag{3.29}$$

The idea is to solve for the constant A that satisfies the volume fraction, where $\phi_{i,j,k}$ is a great initial guess for the value of A. In addition, Equation (3.29) should be rescaled to make it a signed distance function from the interface prior to solving for the constant A.

The constant A requires the solution of the nonlinear equation,

$$F(A) - F_{VOF} = 0\,, \tag{3.30}$$

where F_{VOF} is the volume fraction calculated by the VOF method, and $F(A)$ is the volume fraction corresponding to the value of A. $F(A)$ is a function of the interface orientation and position, which is given by Equation (3.21). The volume fraction, $F(A)$, is calculated by using the techniques outlined in the previous section. It was found that Brent's method worked extremely well for solving Equation (3.30) [Press et. al. (1992)]. The quasi-Newton method and the secant method were found to be unstable; in addition, the bisection method worked, but was slow. Brent's method combines bisection with inverse quadratic interpolation and is guaranteed to converge. Brent's method requires

the root to be bounded, so the maximum and minimum values of the constant A were found geometrically; in addition, the level set value of the cell is a good initial guess for the constant A.

After the constant A is found, the level set value is replaced with the constant A if the cell contains the interface. Then, the level set field away from the interface is reinitialized to a signed distance function from the interface by using the technique suggested by Sussman (1994) (Equation 2.20). It is only necessary to solve Equation (2.20) for approximately 6 steps after each interface reconstruction step to maintain the interface as a signed distance function. The CLSVOF method is quite simple and does not require that much more effort over the traditional VOF method.

3.3.5 Implementing the CLSVOF Scheme

The procedure for implementing the CLSVOF scheme for incompressible flows is to advect the level set field in the first direction and advect the volume fraction field in the same direction using Equation (3.9). The scalar values in Equation (3.9) will correspond to the level set field and the volume fraction field respectively; likewise, the volume fraction values on the faces must be constructed by measuring the exact amount of material leaving the cell. Next, the interface must be reconstructed that satisfies the volume fractions, so solve Equation (3.30) in each cell that contains the interface. After the interface is reconstructed, the level set field is reinitialized to be a signed distance

function from the piecewise linear representation of the interface (Equation 2.20). Now, repeat the process in the next direction.

The procedure for flows with phase change is to advect the level set field (Equation 3.19) in the first direction, then advect the density field (Equation 3.19) in the same direction. The velocity of the level set field corresponds to the interface velocity (Equation 2.8), where the velocity of the density field corresponds to the flow field. Use the density in the cell to calculate the volume fraction (Equation 3.6), and then reconstruct the interface by solving Equation (3.30) in each cell that contains the interface. After the interface is reconstructed, reinitialize the level set field to be a signed distance function from the interface (Equation 2.20). Now, repeat the process for the next direction.

3.4 Initial Value Techniques for Forcing Mass Conservation

Chang et al (1996) and Son (2001) both suggested a different but similar way to force the level set field to globally conserve mass by solving an additional differential equation. Chang et al (1996) suggested solving,

$$\frac{\partial \phi}{\partial \tau} + \left(\hat{M} - M(\phi)\right)(-P + \kappa)\|\nabla \phi\| = 0 \qquad (3.31a)$$

where, $\hat{M}$ is the correct total mass, M is the total mass computed by the level set function ϕ, P is a constant that Cheng set to 1, and κ is the curvature of the interface. The total mass, M, is calculated by the following expression,

$$M(\phi) = \sum_{i,j} \left(\rho_2 + (\rho_1 - \rho_2) H_\varepsilon (\phi_{i,j,k}) \right) \Delta x \Delta y \Delta z \tag{3.31b}$$

Son (2001) suggested solving,

$$\frac{\partial \phi}{\partial \tau} + \left(\hat{V}_k - V_k(\phi) \right) \left\| \nabla \phi \right\| = 0 \tag{3.32}$$

where, $\hat{V}_k$ is the correct total volume of the kth bubble and V_k is the total volume computed by the level set function ϕ of the kth bubble. Son (2001) tracked each bubble region using an indicator function, so that each bubble would conserve volume. The idea is to solve the volume reinitialization equation (Equation 3.31 or 3.32) and the standard distance function reinitialization equation (Equation 2.20) in a predictor-corrector fashion until the mass or volume error is smaller than a specified tolerance.

Equations (3.31) and (3.32) can be written,

$$\frac{\partial \phi}{\partial \tau} + e \left\| \nabla \phi \right\| = 0 \tag{3.33}$$

where *e* represents an artificial velocity which is a function of the volume or mass error. Equation (3.33) can be rewritten to show that the error velocity, *e*, is equal to the characteristic velocity, which is normal to the interface.

$$\frac{\partial \phi}{\partial \tau} + e \frac{\nabla \phi}{\left\| \nabla \phi \right\|} \bullet \nabla \phi = 0 \tag{3.34a}$$

$$\frac{\partial \phi}{\partial \tau} + e \vec{n} \bullet \nabla \phi = 0 \tag{3.34b}$$

The error velocity is projected on the interface in the normal direction, which moves the interface. The idea behind Equation (3.33) is to develop an artificial velocity field corresponding to some volume or mass error that advects the interface to the correct location. Over all, it was found that Equation (3.33) does not converge very well.

Moreover, the error was projected uniformly across the entire interface with the method suggested by Chang et. al. (1996), because the error velocity was a function of the global mass loss. Son (2001) fixed this problem by tracking each region by using an indicator function; however, the technique is cumbersome to use with merging interfaces. A better approach would be to use the volume fraction field.

3.4.1 A New Approach

The level set field should be reinitialized such that it satisfies the local volume fraction field instead of a global constraint, along the lines of the CLSVOF approach. One such approach would be to modify the concepts suggested by Chang et. al. (1996) and Son (2001) and use the volume fraction in the respective cells instead of the total mass of the system (Equation 3.35).

$$\frac{\partial \phi}{\partial \tau} + \left(F_{VOF} - F(\bar{\phi})\right)\|\nabla \phi\| = 0 \tag{3.35}$$

F_{VOF} is the volume fraction that corresponds to the volume of fluid (VOF) method, and $F(\bar{\phi})$ is the volume fraction computed by the linearized level set function $\bar{\phi}$ (Equation 3.22). Unfortunately, Equation (3.35) also did not converge very well, even though the error velocity was a function of the local volume fraction error.

An interesting observation is that the concept behind Equation (3.35) is similar to the interface reconstruction method used with the VOF and CLSVOF schemes. If the time derivative in Equation (3.35) is approximated with a forward difference, then the equation can be written as,

$$\phi^{new} = \phi^{old} - \frac{\Delta x}{2}\left(F_{VOF} - F(\phi^{old})\right)\vec{n} \bullet \nabla\phi^{old} \tag{3.36}$$

where $\Delta\tau = \frac{\Delta x}{2}$ is the maximum stable step size. If ϕ is linearized,

$$\bar{\phi}(x, y, z) = A + (x - x_i)B + (y - y_j)C + (z - z_j)D\,, \tag{3.37}$$

and rescaled such that it is a distance function, $B^2+C^2+D^2=1$, then Equation (3.36) can be written as,

$$A^{new} = A^{old} - \frac{\Delta x}{2}\left(F_{VOF} - F(A^{old})\right). \tag{3.38}$$

where the components of the normal vector were held constant. Equation (3.38) is the simple and slow converging Picard iteration method. The CLSVOF method uses the Brent's method [Press W. H., et al, 1992], which is a root finding technique that converges quickly. The CLSVOF interface reconstruction method and the initial value technique shown by Equation (3.35) are trying to find the root to,

$$F(A) - F_{VOF} = 0\,. \tag{3.39}$$

The formulation shown by Equation (3.35) allows a stronger coupling between the level set field and the volume fraction field, but it does not converge very well.

3.5 Advection Tests

The solid body rotation test was the first test used to determine the accuracy of the CLSVOF scheme. This test involves rotating a notched circle and then comparing the results after one rotation. The domain is $\pi x\ \pi$ with a 100x100 grid, and the circle has

a diameter of $\pi/6$ with a notch that is *10* nodes wide. The velocity field is $u(x,y)=y-\pi/2$ and $v(x,y)=-x-\pi/2$, and one rotation corresponds to 2π seconds. The results from the CLSVOF scheme are compared to the standard level set method. The corners of the notch were numerically smoothed out prior to advecting the circle so that the level set field was approximately a signed distance function from the interface. The results from the notched circle test are shown in Figure (3.4) corresponding to the level set method, the VOF method, and the CLSVOF method. The error norms corresponding to each interface capturing technique are shown in Table (3.1).

The CLSVOF scheme has a 0.7% improvement over the standard PLIC VOF formulation. The LS method did not perform very well when compared to either the VOF or CLSVOF schemes. The LS method tends to smear out the notch where the VOF method can retain the notch. By coupling the LS method with the VOF method, it was possible to capture and preserve the notch. The CLSVOF method produced the best results for the solid body test.

Unlike the standard LS method, the order of accuracy of the directionally split level set advection equation did not affect the accuracy of the CLSVOF scheme. The velocity field with the test problem was divergent free, so the second-order flux construction technique used by Sussman and Puckett (2000) was tested with the CLSVOF method. The difference between the first-order donor cell technique and the second-order technique was insignificant. We suspect the numerical reinitialization technique is limiting the accuracy of the CLSVOF scheme. Sussman and Puckett (2000) reinitialized the level set field to be a signed distance function from the interface exactly,

where in this study we implement the numerical technique [Sussman (1994)] for simplicity.

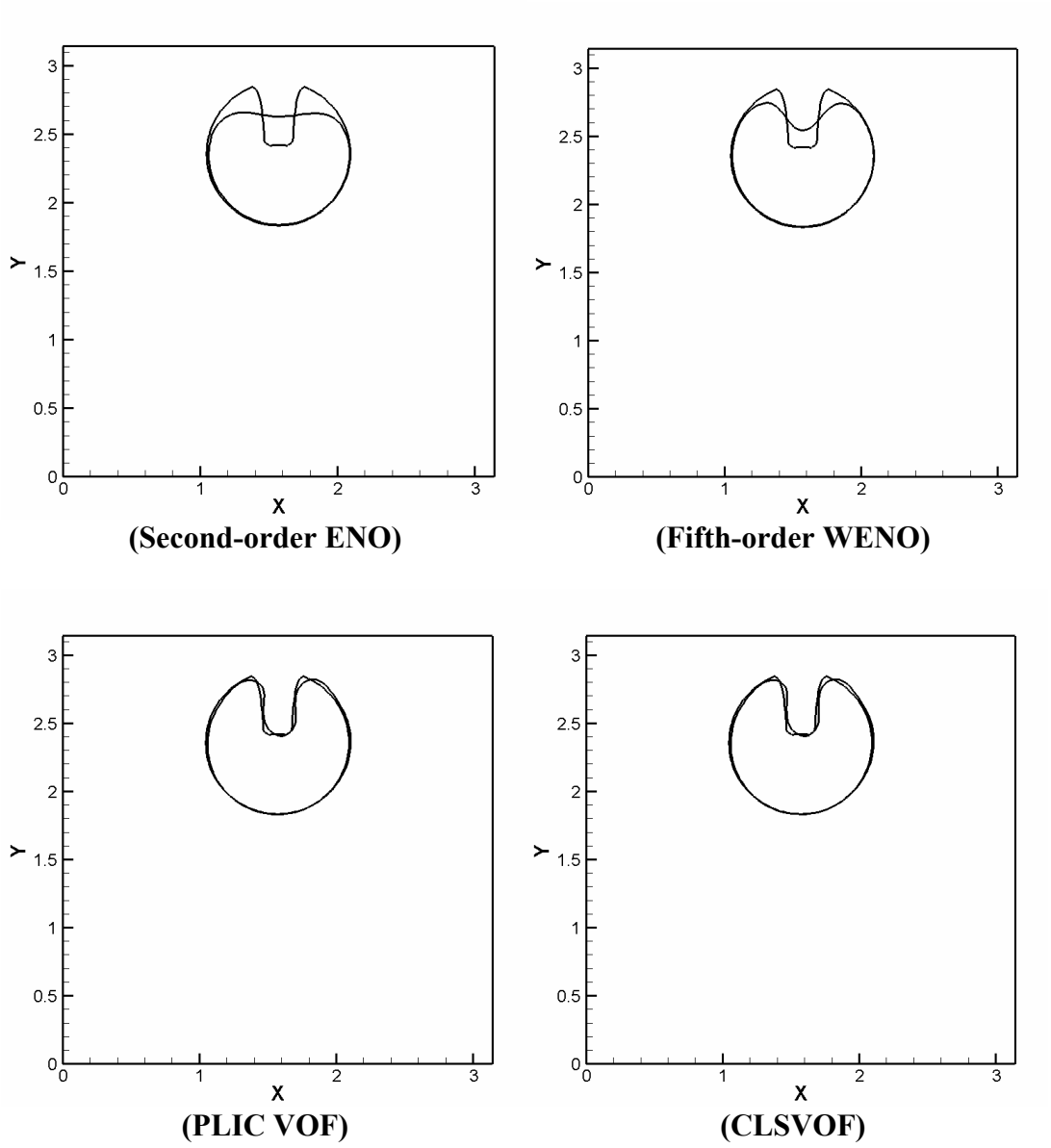

Figure 3.4 The results are shown at the starting location and after 1-rotation, where all the results correspond to a 100x100 mesh.

Table 3.1 The error after 1-rotation

	Error Norm	% Volume Loss
Second-order ENO	1.54 E-02	7.86
Fifth-order WENO	8.60 E-03	2.82
PLIC VOF	4.35 E-03	NA
CLSVOF	4.32 E-03	NA

The second numerical test was the shear flow test. This test involves advecting a circle forward in time a certain number of steps, and then reversing the flow direction and advecting the circle back to the starting location. The domain is $\pi x\ \pi$ with a 100x100 grid, and the circle has a diameter of $\pi/6$. The velocity field is $u(x,y)=\sin(x)*\cos(y)$ and $v(x,y)=\cos(x)\sin(y)$, and the CFL number is 0.5. Tests were conducted with 250, 500, and a 1000 steps. The results for 500 steps are shown in Figure (2.5) corresponding to the level set method, the VOF method, and the CLSVOF method. The error norms corresponding to each interface capturing technique are shown in Table (3.2).

The CLSVOF scheme has identical results to the standard Young's VOF formulation for 1000 steps and slightly better results for 500 steps; however, it has slightly worse results for 250 steps. The LS method had a huge problem with preserving the mass of the circle in the shear flow test. Even with higher-order advection, the LS method lost considerable amounts of volume. By coupling the LS method with the VOF method, the volume loss problem associated with the LS method was fixed.

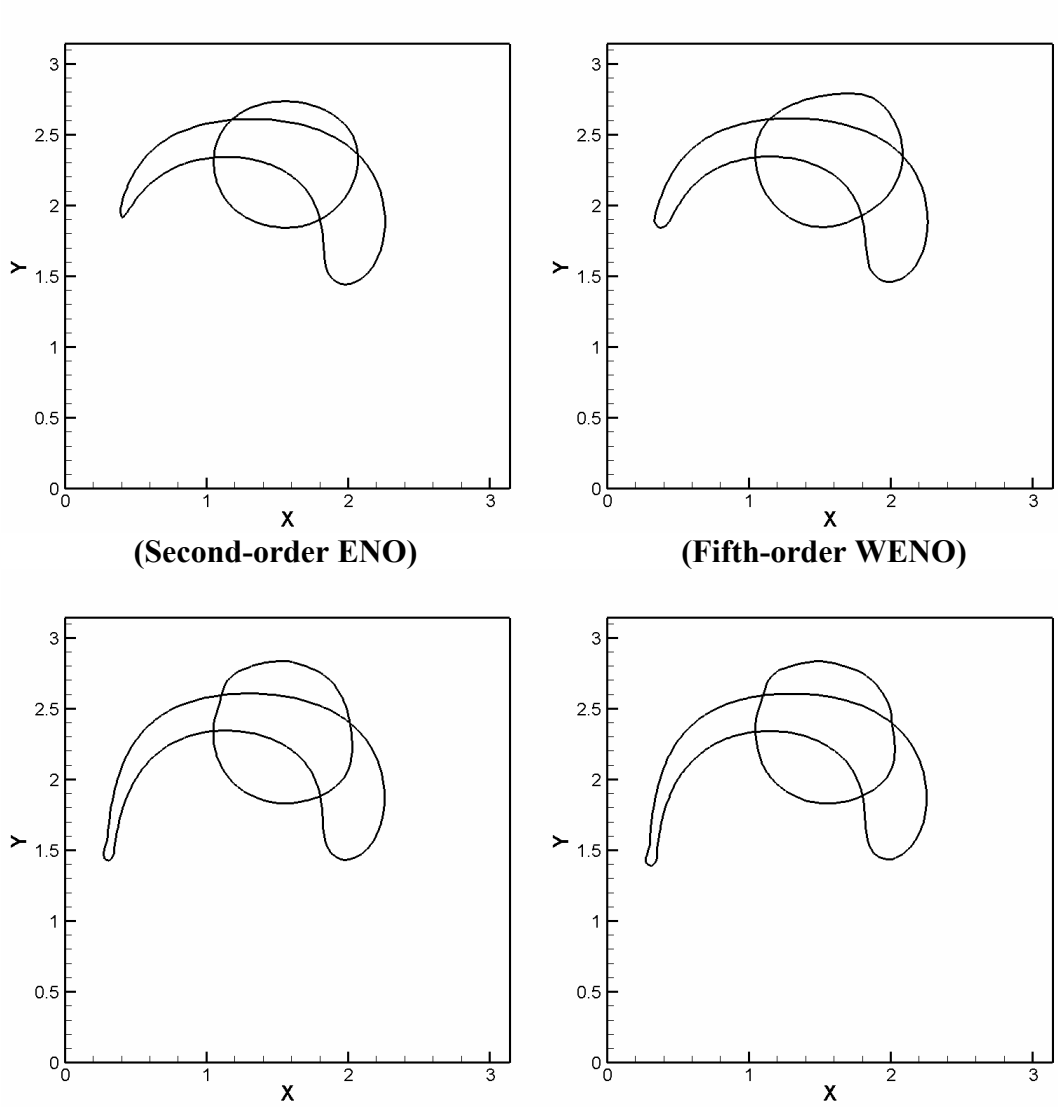

(Second-order ENO) **(Fifth-order WENO)**

(PLIC VOF) **(CLSVOF)**

Figure 3.5 **The results are shown after 500 steps forward in time and when the deformed circle returned to the starting location.**

Table 3.2 The error when the deformed circle returned to the starting location

Steps	250	500	1000
Error Norm	5.39E-03	1.62E-02	4.25E-02
% Volume Loss	6.17	17.86	45.77

(Second-order ENO)

Steps	250	500	1000
Error Norm	2.82E-03	9.34E-03	2.20E-02
% Volume Loss	3.23	10.21	21.93

(Fifth-order WENO)

Steps	250	500	1000
Error Norm	4.34E-03	8.98E-03	3.65E-02

(PLIC VOF)

Steps	250	500	1000
Error Norm	4.36E-03	8.89E-03	3.65E-02

(CLSVOF)

3.6 Droplet Test

The performance of the CLSVOF scheme was tested by modeling a liquid drop falling into a pool. The results from the droplet impact at several different times are shown in Figure (3.6), where the level set (LS) method corresponds to the dashed line, and the CLSVOF method corresponds to the solid line. The CLSVOF method appears to preserve the fine scale features where the LS method tended to smear out the sharp features. In addition, the CLSVOF method appears to capture the fragmentation of the interface, and the air entrained from the impact. Coupling the VOF method with the LS method appears to substantially improve the accuracy of the results, based on an observational assessment.

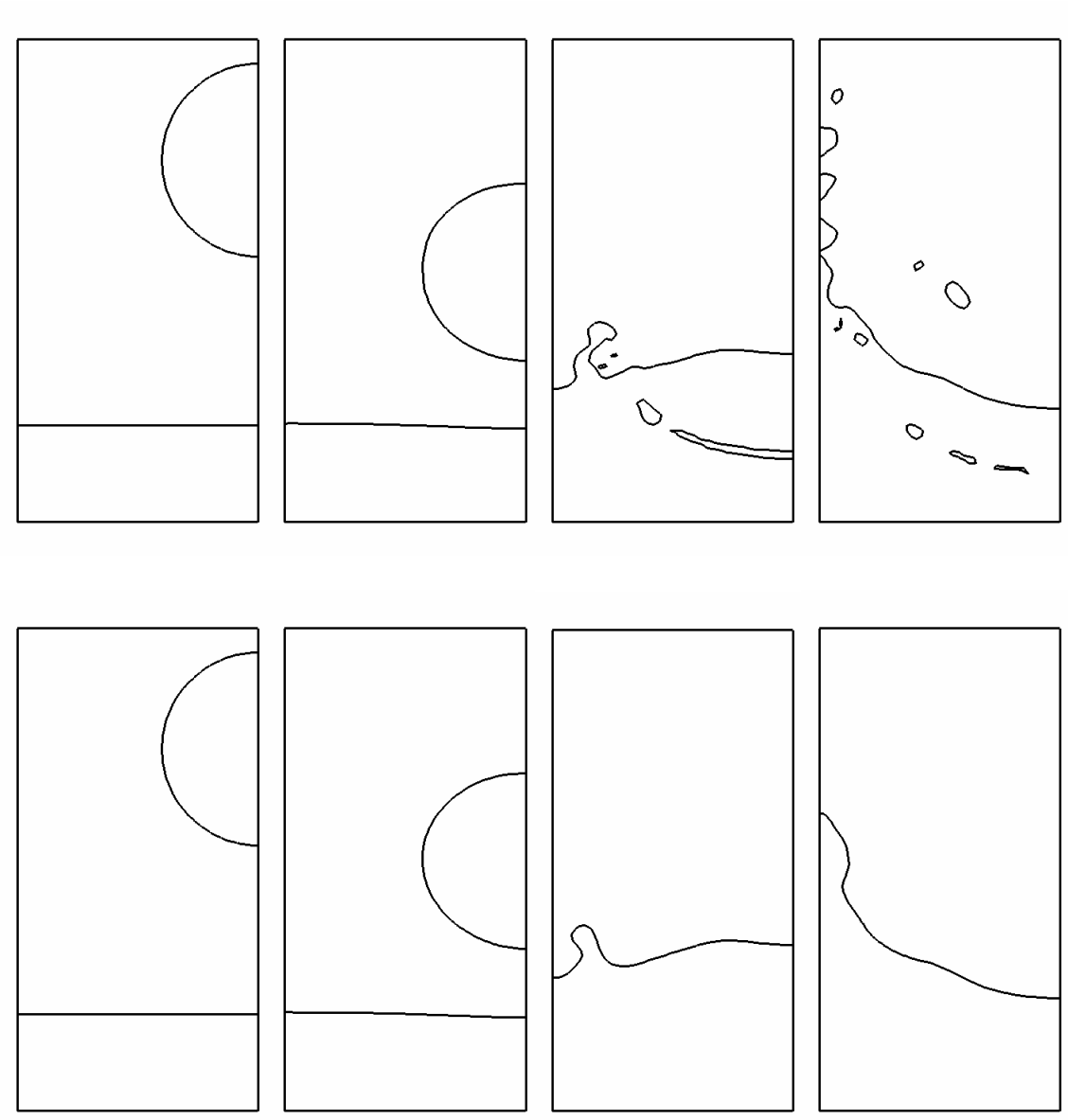

Figure 3.6 **Droplet test results corresponding to the CLSVOF method (top row) and the level set method (bottom row).**

3.7 Film Boiling

The film boiling method outlined in the previous chapter can be adapted to work with the CLSVOF technique. The level set field must be advected at the interface velocity; thus, the temperature gradients must be known on the cell faces. As a result, the temperature gradients were extrapolated to the cell faces. In addition, the temperature gradients on the interface did not use the ghost nodes. The properties used for the film boiling simulation are shown in Table (2.1). In addition, the boundary conditions and initial conditions are identical to the saturated film boiling test problem in section (2.11).

The film boiling results corresponding to the CLSVOF scheme and the level set method are shown in Figure (3.7) at 0, 0.2, 0.25, and 0.3 seconds. The level set method had a tendency to smooth out the sharp features where the CLSVOF scheme preserved them. Based on the tests performed in this study, the CLSVOF scheme produces results that are superior to the standard level set method.

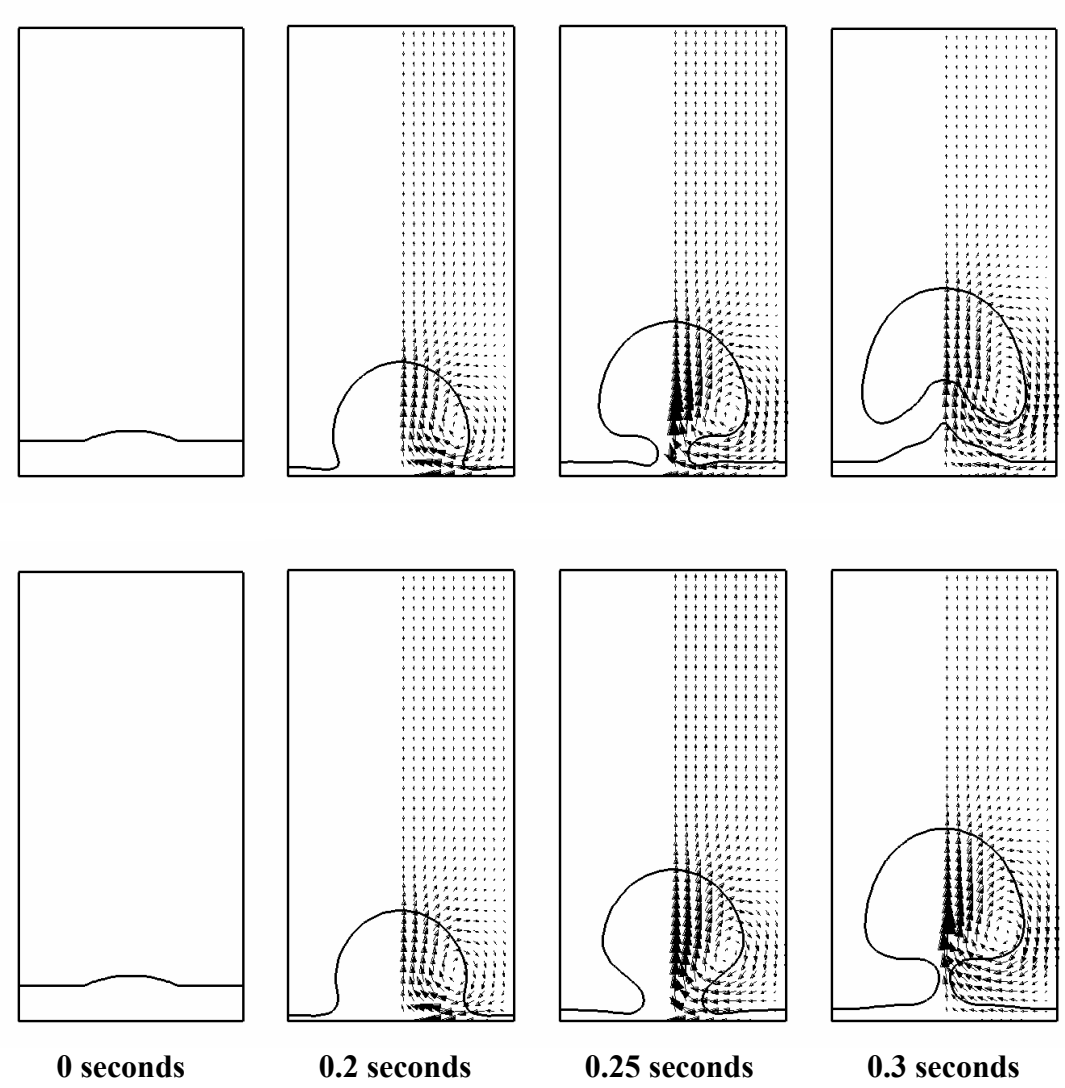

Figure 3.7 **Film boiling test results corresponding to the CLSVOF method (top row) and the level set method (bottom row).**

CHAPTER 4
CONCLUSION

4.1 Phase Change Scheme

The liquid-vapor phase transition technique presented in this thesis offers a simple way to model boiling flows and condensation while accounting for both latent heat and different material properties. The concept behind the new technique is to treat each phase as incompressible except along the interface. The continuity equation is modified to account for the volume change that occurs along the interface by adding a source term to the right hand side. The continuity equation source term is calculated by solving the Rankine-Hugoniot jump conditions. Then, another source term is added to the energy equation to account for the latent heat that is released or absorbed. However, the energy equation source term is not explicitly determined; instead, the energy equation source term is satisfied by solving an extrapolation equation in an iterative fashion that forces the temperature in the neighboring cells to correspond to the interface boundary condition. In addition, this iterative methodology captures the discontinuous temperature gradients across the interface. Likewise, the temperature gradients on the interface are calculated by propagating ghost points into the respective phase; this allows the interface to be treated in a sharp manner for the source term in the continuity equation.

The remaining parts of this multiphase simulation are accomplished using standard techniques. The surface tension force is modeled by adding a source term to the momentum equation, which distributes the effect of the surface tension over three nodes

along the interface. This approach to modeling surface tension is commonly referred to as the standard continuous surface force model. The continuous surface force model allows the pressure to be calculated using standard single phase Navier-Stokes solvers. In this study, the projection technique is used to solve the Navier-Stokes equations and the interface location is captured by the level set method. Finally, the standard level set reinitialization method and the coupled level set volume of fluid (CLSVOF) reinitialization method are used to complete the simulation in this study.

Several numerical tests were performed with the new phase transition scheme. The first test involved modeling a one-dimensional phase transition problem and then comparing the numerical results to the analytical solution. Likewise, the next numerical test was a two-dimensional phase transition problem that had an analytical solution. The results from the one- and two-dimensional phase transition problems demonstrated that the new phase transition method is second-order accurate. The final test involved modeling an actual film boiling problem and then comparing the results to the Berrenson correlation. The results from the film boiling problem agreed fairly well with the Berrenson correlation. Based on this research, the new phase transition method will enhance the modeling capabilities of the level-set method and assist in answering questions in multiphase problems.

4.2 Improving the Level Set Method

Several techniques have been suggested for fixing the mass loss problem associated with the level set method. The first correction technique involves solving an initial value problem, and the second correction technique involves coupling the level set method with the volume of fluid method (CLSVOF). In this work, both of these correction techniques were studied. In addition, the CLSVOF method was extended to work with flows that have phase change, and comparisons were made between the new advection scheme and the standard level set method. Multiple comparison studies were performed in this work with incompressible and boiling flows.

The initial value techniques correct the mass loss problem by projecting the error at each iteration onto the interface. The error is transformed into an artificial velocity that moves the interface to a location that satisfies global or regional mass conservation as the solution approaches steady state in artificial time. One problem with the current initial value techniques is the artificial velocity is a function of the entire flow field or the respective bubble, so the error is distributed uniformly over the entire interface. Another problem is that these initial value techniques have slow convergence rates. In an attempt to remedy these problems, another initial value approach was investigated that used the difference in the volume fraction in each cell to formulate an artificial velocity that depended on the local conditions. The volume fraction difference was based on the PLIC VOF approach and the level set method. However, it was found that this initial value technique also had a poor convergence rate. Moreover, it was found that this

initial value technique was based a Picard iteration, which is known for slow convergence; whereas, the CLSVOF method uses a faster converging technique.

The next mass correction technique studied was the CLSVOF method. The CLSVOF approach uses the PLIC VOF method to determine the correct volume fraction in each cell. Then, the level set field is reinitialized to (1) satisfy the volume fraction in each cell, and (2) be a signed distance function from the interface. The CLSVOF method was found to be substantially more accurate than the level set method with fifth-order WENO advection. The advection tests illustrate that the level set method will smooth out sharp features, while the CLSVOF method will preserve them. In the droplet impact test, the CLSVOF method captured the air entrained in the form of bubbles, whereas, the level set method deleted this feature. Based on these comparison studies, the CLSVOF method was extended to work with flows that have phase change. Then, a film boiling simulation was performed to compare the results of the CLSVOF advection scheme with the level set method. It was found that the CLSVOF method captured the narrow neck of the vapor plume, whereas, the level set method smoothed-out this feature. In addition, the level set method smoothed-out the smaller vapor bubbles. Coupling the level set method with the VOF method works extremely well and is fairly efficient.

4.3 Contributions to Existing Numerical Techniques

This research effort has resulted in the development of a new liquid-vapor phase transition technique. The new technique accounts for different material properties in the

respective phases such as specific heat, which is an improvement over previous level set phase transition methods. In addition, a new method was presented for maintaining the interface at the saturation temperature. The concept behind the new method is to solve an extrapolation equation along the interface to determine the temperature in the neighboring nodes that corresponds to the interface boundary condition. Likewise, the extrapolation equation was modified to construct ghost nodes along the interface, which were used to capture the discontinuous temperature gradients across the interface. One of the current ghost node construction approaches involves solving a first-order wave equation; however, this approach does not account for the temperature gradient. The new ghost node construction method accounts for the temperature gradient and the method implicitly accounts for the interface boundary condition, so this approach was found to be more accurate.

The second portion of this research focused on resolving the mass loss problem of the level set method, and this portion of the research resulted in the development of a new level set advection algorithm for phase transition flows. Several techniques were studied for fixing the mass loss problem, and it was found that the coupled level set volume of fluid (CLSVOF) approach performed better than the initial value techniques. As a result, a new CLSVOF method was developed that uses the new phase transition technique. In summary, this research has developed (1) a new liquid-vapor phase transition model that accounts for different material properties, (2) a new extrapolation technique for satisfying the interface boundary conditions, (3) a new ghost node construction technique, and (4) a new CLSVOF method for modeling flows with phase transition. In addition, a comparison study was conducted with the CLSVOF method

and the standard level set method. The CLSVOF method was also compared to several initial value techniques.

4.4 Future Work

In some liquid-vapor phase transition problems, the saturation temperature is highly dependent on the pressure. In an attempt to account for this effect, the saturation temperature was made a function of the pressure. Then, a loop was constructed that included the procedure for satisfying the interface boundary condition, the ghost node construction process, and the pressure Poisson equation (PPE) solver. It was found that the continuity equation source term, which is on the right hand side of the PPE, would continue to increase in size; therefore, the pressure would blow up. A technique needs to be developed that prevents the pressure from blowing up. The approach suggested in this thesis for satisfying the interface boundary conditions offers a potential framework for handling the effect of pressure on the saturation temperature.

Another important extension of this research is to model three-dimensional boiling problems. In this study, only two-dimensional tests were conducted due to memory and speed constraints. The extrapolation equations used for satisfying the interface boundary condition and constructing ghost nodes should work in three-dimensions. In addition, it would be advantageous to parallelize the new phase transition scheme.

APPENDIX A
HIGHER-ORDER EXTRAPOLATION

Equations (A1a) through (A1c) correspond to an interpolation scheme that is constructed from Second-order forward and backward differences. Change the sign on the level set function in Equations (A1b) and (A1c) for a higher-order ghost node construction method.

$$T_{i,j} = \frac{T_{SAT} - B}{A} \tag{A1a}$$

where,

$$A = 1 + \frac{3}{2}\left(- \frac{\min(0,-\phi_{i,j} n_{i,j}^{x})}{\Delta x} + \frac{\max(0,-\phi_{i,j} n_{i,j}^{x})}{\Delta x} - \frac{\min(0,-\phi_{i,j} n_{i,j}^{y})}{\Delta y} + \frac{\max(0,-\phi_{i,j} n_{i,j}^{y})}{\Delta y} \right) \tag{A1b}$$

$$B = \frac{1}{2}\left(\frac{\min(0,-\phi_{i,j} n_{i,j}^{x})}{\Delta x}\left(4T_{i+1,j} - T_{i+2,j}\right) - \frac{\max(0,-\phi_{i,j} n_{i,j}^{x})}{\Delta x}\left(4T_{i-1,j} - T_{i-2,j}\right) + \frac{\min(0,-\phi_{i,j} n_{i,j}^{y})}{\Delta y}\left(4T_{i,j+1} - T_{i,j+2}\right) - \frac{\max(0,-\phi_{i,j} n_{i,j}^{y})}{\Delta y}\left(4T_{i,j-1} - T_{i,j-2}\right) \right). \tag{A1c}$$

The level set function is defined as less than zero inside the interface and greater than zero outside the interface; as a result, the normal vector points away from the interface. If the normal vector points in the opposite direction (into the vapor), then the negative sign in front of the normal vector must be deleted.

REFERENCES

Bajan, A., Advanced Engineering Thermodynamics, John Wiley & Sons, New York, pp. 263-264 (1997).

Balaras, E., "Modeling Complex Boundaries using an External Force Field on Fixed Cartesian Grids in Large-Eddy Simulations," *Computers & Fluids*, Vol. 33, pp. 375-404 (2004).

Bourlioux, A., "A Coupled Level-Set Volume-of-Fluid Algorithm for Tracking Material Interfaces," *Proc. 6th Int. Symposium on Computational Fluid Dynamics*, Lake Tahoe, CA, pp. 15-22, (1995).

Brackbill, J.U., Kothe, D.B., and Zemach, C., *A Continuum Method for Modeling Surface Tension*, Journal of Computational Phys. Vol. 100, pp. 335-354 (1992).

Chang, Y. C., Hou, T. Y., Merriman, B., and Osher S., "A Level Set Formulation of Eulerian Interface Capturing Methods for Incompressible Fluid Flows", *Journal of Computational Physics*, Vol. 124, pp. 449-464, (1996).

Collier, J.G., and Thome J.R., Convective Boiling and Condensation, 3rd ed., Oxford Science Publications, New York, pp. 168-169 (1996)

Chorin, A., "Numerical Solution of the Navier-Stokes Equations", Math. Comp. 22, pp. 745-762 (1968).

Fedkiw, R.P, Aslam, T., Merriman, B., and Osher, S., "A Non-oscillatory Eulerian Approach to Interfaces in Multimaterial Flows (the Ghost Fluid Method)," *Journal of Computational Physics*, Vol. 152, pp. 457-492 (1999).

Gibou, F., Fedkiw, R., Caflisch, R., and Osher, S., "A Level Set Approach for Numerical Simulation of Dendritic Growth," *Journal of Scientific Computing*, Vol. 19, pp. 183-199 (2003).

Gilmanov, A., Sotiropoulos, F., and Balaras, E., "A General Reconstruction Algorithm for Simulating Flows with Complex 3D Immersed Boundaries on Cartesian Grids," *Journal of Computational Physics*, Vol. 191, pp. 660-669 (2003).

Golub G. H., and Van Loan C. F., Matrix Computations, The John Hopkins University Press, Baltimore, MA pp. 363-379 (1983)

Harlow, F. H., and Welch, J. E., "Numerical calculation of time-dependent viscous incompressible flow of fluid with free surface." *Physics of Fluids*, Vol. 8, pp. 2182-2189 (1965)

Hirt, C. W., and Nichols, B. D., "Volume of Fluid (VOF) Method for the Dynamics of Free Boundaries," *Journal of Computational Physics*, Vol. 39, pp. 201-225, (1981).

Jiang, G.-S., and Peng, D., "Weighted ENO Schemes for Hamilton Jacobi Equations," *SIAM Journal of Scientific Computing*, Vol. 21, pp. 2126-2143 (2000).

Juric, D., and Tryggvason, G., "A Front Tracking Method For Dendritic Solidification," *Journal of Computational Physics*, Vol. 123, pp.127-148 (1996).

Juric, D., and Tryggvason, G., "Computations of Boiling Flows," *International Journal of Multiphase Flow*, Vol. 24, No.3, pp.387-410 (1998).

Kang, M., Fedkiw, R.P, and Liu, X., "A boundary Condition Capturing Method for Multiphase Incompressible Flow," *Journal of Scientific Computing*, Vol. 15, No. 3 (2000)

Kelley, C. T., Iterative Methods for Linear and Nonlinear Equations, SIAM, Philadelphia pp. 11-29 (1995)

Liu, X., Fedkiw, R.P, and Kang, M., "A Boundary Condition Capturing Method for Poisson's Equation on Irregular Domains," *Journal of Computational Physics*, Vol. 160, pp. 151-178 (2000)

Noh, W. F., and Woodward, P., "SLIC (simple line interface calculation)," *Lecture Notes in Physics*, edited by A. I. Van Dooren and P. J. Zandbergen, Vol. 59, Springer, New York, pp. 330-340, (1976).

Osher, S., and Fedkiw, R.P., "Level Set Methods: An Overview and Some Recent Results," *Journal of Computational Physics*, Vol. 169, pp. 463-502 (2001).

Osher, S., and Fedkiw, R.P., Level Set Methods and Dynamic Implicit Surfaces, Springer, New York (2003).

Osher, S., and Sethian, J., "Fronts Propagating with Curvature Dependent Speed: Algorithms Based on Hamilton-Jacobi Formulations," *Journal of Computational Physics*, Vol. 79, pp. 12-49 (1988).

Özişik, M.N., Heat Conduction 2nd Edition, John Wiley & Sons Inc., New York, pp. 404-408 (1993).

Peskin, C., *Numerical Analysis of Blood Flow in the Heart*, Journal of Computational Physics, Vol. 25, pp. 220-252 (1977).

Press, W. H., Teukolsky, S, A., Vetterling, W. T., Flannery, B. P., Numerical Recipes in Fortran 77 2nd Edition, Press Syndicate, New York, NY, pp 352-355 (1992).

Puckett, E. G., "A Volume-of-Fluid Interface Tracking Algorythm with Applications to Computing Shock Wave Refraction," *Proceedings, 4th International Symposium on Computational Fluid Dynamics*, Davis, CA, edited by H. Dwyer, p. 933 (1991).

Puckett, P. G., Almgren, A. S., Bell, J. B., Marcus, D. L., and Rider, W. J., "A High-Order Projection Method for Tracking Fluid Interfaces in Variable Density Incompressible Flows," *Journal of Computational Physics*, Vol. 130, pp. 269-282, (1997).

Rider, W. J., and Kothe, D. B., "Reconstructing Volume Tracking," *Journal of Computational Physics*, Vol. 141, pp. 112-152, (1998).

Rudman, M., "Volume-Tracking Methods for Interfacial Flow Calculations," *International Journal for Numerical Methods in Fluids*, Vol. 24, pp. 671-691, (1997).

Sethian, J.A., Level Set Methods and Fast Marching Methods, Cambridge University Press, Cambridge (1999).

Shin, S., and Juric, D., "Modeling Three-Dimension Multiphase Flow Using a Level Contour Reconstruction Method for Front Tracking without Connectivity," *Journal of Computational Physics*, Vol. 180, pp. 427-470 (2002).

Son, G., "A Numerical Method For Bubble Motion with Phase Change," *Numerical Heat Transfer, Part B.*, Vol. 39, pp. 509-523, (2001).

Son, G., "Efficient Implementation of a coupled Level-Set and Volume-Of-Fluid Method for Three-Dimensional Incompressible Two-Phase Flows," *Numerical Heat Transfer, Part B.*, Vol 43, pp. 549-565, (2003).

Son, G., and Dhir, V.K., "Numerical Simulation of Film Boiling Near Critical Pressures with a Level Set Method," *J. Heat Trans.* Vol. 120, pp. 183-192 (1998).

Son, G., Dhir, V.K., Ramanujapu, N., "Dynamics of Heat Transfer Associated with a Single Bubble During Nucleate Boiling on a Horizontal Surface," *J. Heat Trans.* Vol. 121, (1999).

Sussman, M., Puckett E, G., "A Coupled Level Set and Volume-of-Fluid Method for Computing 3D and Axisymmetric Incompressible Two-Phase Flows," *Journal of Computational Physics*, Vol. 162, pp. 301-337 (2000).

Sussman, M., "A second order coupled level set and volume-of-fluid method for computing growth and collapse of vapor bubbles," *Journal of Computational Physics*, Vol. 187, pp. 110-136 (2003).

Sussman, M. and Fatemi, E., "An efficient Interface Preserving Level Set Redistancing Algorithm and its Application to Interfacial Incompressible Fluid Flow," SIAM *Journal of Scientific Computing*, Vol. 20, num. 4., pp. 1165-1191 (1999).

Sussman, M., Smereka, P. and Osher, S.J., "A Level Set Method for Computing Solutions to Incompressible Two-Phase Flow," *Journal of Computational Physics*, Vol. pp. 146-159 (1994).

Torres, D., and Brackbill, J., "The Point-Set Method: Front-Tracking without Connectivity," *Journal of Computational Physics*, Vol. 165, pp. 620-644 (2000)

Tryggvason, G., Bunner, B., Esmaeeli, A., Juric, D., Al-Rawahi, A., Tauber, W., Han, J., Nas, S., Jan, Y.J., "A Front-Tracking Method for the Computations of Multiphase Flow," *Journal of Computational Physics*, Vol. 169, pp. 708-759 (2001).

Welch, S.W.J., and Wilson, J., *A Volume of Fluid Based Method for Fluid Flows with Phase Change*, Journal of Computational Physics, Vol. 106, pp. 662-682 (2000).